TECHNICAL NOTE

D-1051

APPLICABILITY OF MIXING LENGTH THEORY TO A

TURBULENT VORTEX SYSTEM

By Robert G. Ragsdale

Lewis Research Center
Cleveland, Ohio

NATIONAL AERONAUTICS AND SPACE ADMINISTRATION

WASHINGTON   August 1961

E-1145

NATIONAL AERONAUTICS AND SPACE ADMINISTRATION

———————————

TECHNICAL NOTE D-1051

———————————

APPLICABILITY OF MIXING LENGTH THEORY TO A TURBULENT VORTEX SYSTEM

By Robert G. Ragsdale

SUMMARY

The ability of mixing length theory to correlate vortex data is evaluated. Expressions are derived for eddy diffusivity by applying the techniques of von Kármán and Prandtl which have been established for pipe flow. Total and static pressures were measured from the outer radius to the exhaust-nozzle radius of a vortex generator for a range of mass flows. These data are combined with Navier-Stokes solutions for this region of a compressible vortex to determine turbulent Reynolds numbers. The Reynolds number is related to Prandtl and Kármán functions for various assumed boundary conditions, and the experimental data are used to determine the usefulness of these expressions. The following conclusions were reached:

(1) Mixing length functions developed by applying von Kármán's similarity hypothesis to vortex motion correlate the data better than do Prandtl functions obtained with the assumption that mixing length is proportional to radius.

(2) Some of the expressions developed do not adequately represent the experimental data.

(3) The data are correlated with acceptable scatter by evaluating the fluid radial inertia at the outer boundary and the shear stress at the inner boundary. The universal constant κ was found to be 0.04 to 0.08, rather than the value of 0.4 which is accepted for rectilinear flow.

(4) The data are best correlated by a modified Kármán expression which includes an effect of radial inertia, as well as shear stress, on eddy diffusivity.

INTRODUCTION

The hydrodynamics of vortex flow has been the subject of a number of technical reports. The initial interest in vortex flow was associated with the energy separation, or Ranque-Hilsch effect, which is still under

investigation. Hartnett and Eckert (ref. 1) have reported measurements of temperature and velocity profiles in a Ranque-Hilsch tube for a range of conditions. Their data were taken at various axial distances from the vortex inlet region. More recent data (ref. 2) suggest that the energy separation is effected in the vortex generator itself and that the axial discharge tubes are not a requirement for the Ranque-Hilsch phenomenon. In an extensive analysis of velocity, temperature, and pressure distributions in a turbulent vortex with radial and axial flow, reference 3 concludes that the most important factor affecting the energy separation in a compressible vortex is the turbulent shear work done on or by a fluid element.

By applying the results of an analysis of a viscous vortex to meteorological data of tornado dimensions, it was found that the assumption of turbulence resulted in reasonable agreement with observed sizes (ref. 4). It is pointed out that the turbulence should diminish as the fluid accelerates toward the center, but that in the core the reverse effect may well exist. Reference 4 suggests as a possible generalization that the eddy viscosity be taken as proportional to exponential powers of tangential velocity and fluid kinematic viscosity.

A number of analyses of vortex systems have utilized the assumption of laminar flow. The case of a compressible, viscous, heat-conducting vortex flow generated by a rotating cylinder in an infinite fluid field has been treated in reference 5. From an analysis of the heat transfer in a system of a dissociating gas in vortex flow between two concentric cylinders, reference 6 found that the amount of energy that can be transported is greatly dependent on the radial Reynolds number. Reference 7 has considered the case of magnetohydrodynamically driven vortices and the reverse condition of an ionized gas in vortex flow generating electrical power. The indicated performance of these systems, of course, is dependent on the assumed condition of laminar flow.

Vortex flow is also receiving current attention as a device to permit the use of a gaseous nuclear reactor as a rocket motor. It is readily shown that the practical operation of such a reactor requires that the holdup time of the fissionable gas be increased to 100 to 1000 times that of the propellant, and a vortex field suggests itself (ref. 8) as a possible means of attaining such a flow condition. In this system, turbulence plays a double role. It diminishes maximum tangential velocities, and, more importantly, it seriously limits the rate at which the propellant gas can diffuse through the fuel region. The results of an analysis of an air-bromine vortex system (ref. 9) show the degree to which turbulence limits the maximum concentration of the heavy gas in such a system. Experimental data are also given which indicate that the vortex flow is turbulent. Two recent studies of a vortex gaseous reactor are reported in references 10 and 11.

In each of these instances of vortex flow, the need for an understanding of turbulence is apparent. Analyses based on laminar flow are indeed useful as a means of establishing ideal system performance. As in pipe flow, however, a knowledge of the turbulent regime becomes necessary in order to predict performance characteristics encountered in most practical situations. It has been suggested that Prandtl's mixing length theory (ref. 12) or von Kármán's similarity hypothesis (ref. 3) could be applied successfully to a turbulent vortex. Since these techniques have been substantiated for rectilinear flow, this would seem to be a reasonable approach.

It is not so clear, however, how specifically to apply either of these techniques to vortex flow. It becomes necessary, therefore, to obtain experimental data for turbulent vortex flow and then to evaluate the validity of a mixing length type of approach to such a system. This has been done, and the results are presented herein.

An analytical expression for the radial variation of tangential velocity is obtained by replacing the laminar viscosity in the Navier-Stokes equations by an eddy viscosity which is assumed to be invariant with radial position. Turbulent Reynolds numbers were determined for the flow of air through a vortex generator by matching the analytical expression for tangential velocity with measured values at two radial stations. By using both Prandtl and Kármán techniques and various assumed boundary conditions, expressions are developed which give the turbulent Reynolds number as a function of radial and tangential velocities. These expressions were then investigated in terms of their ability to correlate the experimental data.

Some of the functions did correlate the data with reasonable scatter; some did not. By using a modification of von Kármán's basic approach that was indicated by a trend of the data, a new function was derived. This new expression is related to basic vortex flow parameters and is shown to best correlate the experimental data. While the numerical values of the constants in this function may not be applicable to vortices of different geometries, it is felt that the correlation does properly suggest a general functional relation of parameters affecting vortex flow.

SYMBOLS

a	numerical constant
C	constant in eq. (11)
C_0, C_1, C_2	numerical constants
c_p	specific heat at constant pressure

D   vortex outer diameter, $2r_o$

E_m eddy viscosity

g   gravitational constant

J   mechanical equivalent of heat

k   thermal conductivity

L   vortex axial length

l mixing length

M   molecular weight

P   total pressure

P*   pressure parameter defined in eq. (42)

p   static pressure

R   gas constant

Re   radial Reynolds number

r   radius

T   total temperature

t   static temperature

u   radial velocity

v   tangential velocity

w   weight flow

y   distance from wall

z   axial coordinate

γ ratio of specific heats

ϵ eddy diffusivity

θ angular coordinate

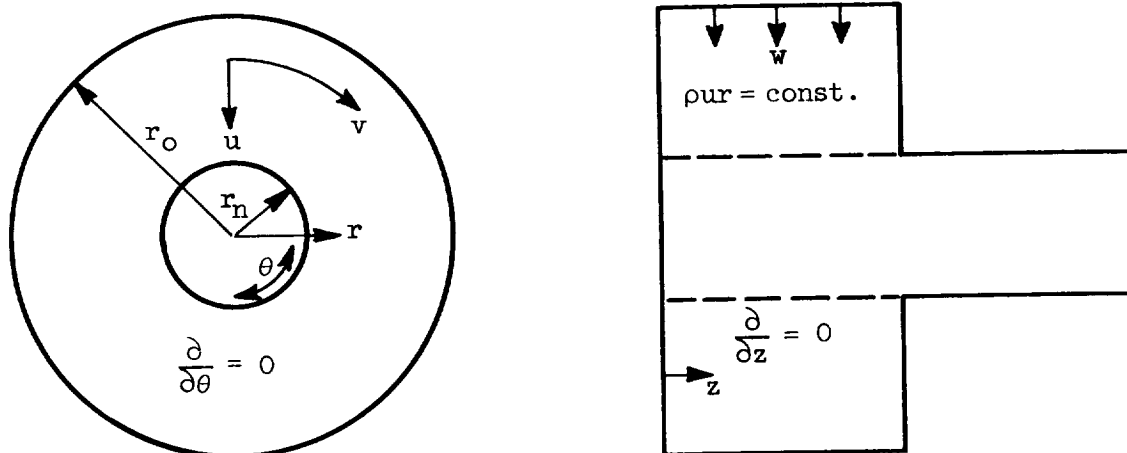|	
κ	universal constant in mixing length theory
μ	viscosity
ρ	density
τ	shear stress
Φ	dissipation term in energy equation
ψ_1, ψ_2, ψ_3	viscous correction factors

Subscripts:

l	laminar
n	inner or nozzle
o	outer
t	turbulent
∞	infinity

Superscript:

'	normalized to value at r_n

ANALYSIS

The general nomenclature for the analysis is as indicated in the following sketch:

Vortex analytical model

Assumptions

The assumptions made throughout the analysis are listed here, but not necessarily in order of occurrence or importance:

(1) Thermal conductivity is zero

(2) $\partial/\partial\theta = \partial/\partial z = 0$ (only the annular region is considered)

(3) Steady state

(4) The perfect gas law is obeyed

(5) No external body forces

(6) $u \ll v$, $du/dr \ll dv/dr$

(7) μ and $\rho\epsilon$ are constant

(8) Turbulent flow can be represented by laminar relations if μ is replaced by $\rho\epsilon$

(9) Radial and tangential velocity fluctuations are equal.

Fundamental Relations of Vortex Flow

Basic equations. - The technique described herein to determine the turbulent Reynolds number of vortex flow from experimental measurements is reported in reference 9. To obtain closed-form solutions for vortex flow, laminar equations are used and then, by virtue of assumption (8), are applied to the turbulent regime. The equations which require that the system conserve fluid momentum are the Navier-Stokes relations (ref. 13). For compressible viscous flow and $\partial/\partial\theta = \partial/\partial z = 0$, they may be written:

$$\rho u \frac{\partial u}{\partial r} - \rho \frac{v^2}{r} = - \frac{\partial p}{\partial r} + \frac{\partial}{\partial r}\left\{\mu\left[2 \frac{\partial u}{\partial r} - \frac{2}{3r} \frac{\partial(ru)}{\partial r}\right]\right\} + \frac{2\mu}{r}\left(\frac{\partial u}{\partial r} - \frac{u}{r}\right) \quad (1)$$

$$\rho u \frac{\partial v}{\partial r} + \rho u \frac{v}{r} = \frac{\partial}{\partial r}\left[\mu\left(\frac{\partial v}{\partial r} - \frac{v}{r}\right)\right] + \frac{2\mu}{r}\left(\frac{\partial v}{\partial r} - \frac{v}{r}\right) \quad (2)$$

The conservation of system energy for zero thermal conductivity is:

$$(\rho u c_p)\frac{\partial t}{\partial r} - u \frac{\partial p}{\partial r} = \Phi = \mu\left[2\left(\frac{\partial u}{\partial r}\right)^2 + 2\left(\frac{u}{r}\right)^2 + \left(\frac{\partial v}{\partial r} - \frac{v}{r}\right)^2 - \frac{2}{3}\left(\frac{\partial u}{\partial r} - \frac{u}{r}\right)^2\right] \quad (3)$$

The continuity equation for steady-state flow in the annular region $(r_n < r < r_o)$ is:

$$\frac{\partial(\rho u r)}{\partial r} = 0 \qquad (4)$$

Finally, the equation of state is:

$$p = \frac{\rho R t}{M} \qquad (5)$$

Ideal fluid relations. - For an ideal fluid ($\mu = 0$) and the assumption that radial velocity functions are small compared with corresponding tangential ones, the following familiar relations are obtained from equations (1) to (5):

$$P = p\left(1 + \frac{\gamma - 1}{2}\frac{Mv^2}{\gamma_g R t}\right)^{\frac{\gamma}{\gamma-1}} = \text{const.} \qquad (6)$$

$$T = t\left(\frac{P}{p}\right)^{\frac{\gamma-1}{\gamma}} = \text{const.} \qquad (7)$$

$$v = \frac{v_o r_o}{r} \qquad (8)$$

$$-\rho u r = \frac{w}{2\pi L} = \text{const.} \qquad (9)$$

Since the continuity relation expressed by equation (4) is for the annular region of the vortex, where $\partial/\partial z = 0$, equation (9) is similarly restricted. The negative sign in equation (9) arises because the flow is radially inward. Equations (6) to (9), though useful as simple approximations, become less and less valid as higher vortex strengths are considered and are useful only for comparing real conditions with ideal ones.

Real fluid relations. - By using equation (9) and the boundary condition $v(r_o) = v_o$, equation (2) may be integrated to give the tangential velocity profile:

$$v' = \frac{v_o' r_o'}{r'}\sqrt{\psi_1} \qquad (10)$$

8

where

$$\psi_1 \equiv \left(\frac{1}{v_o' r_o'}\right)^2 \left[(1 - C)^2 + 2 \frac{C - C^2}{(r')^{Re-2}} + \frac{C^2}{(r')^{2Re-4}}\right] \tag{11}$$

Here, a laminar Reynolds number is defined in terms of radial velocity:

$$Re_l \equiv - \frac{\rho u r}{\mu} \tag{12}$$

In equations (10), (11), and all succeeding ones the prime superscript refers to the quantity normalized to its value at the radius r_n; this is, analytically, the smallest radius at which equation (4) applies and, numerically, is taken to be the exhaust-nozzle radius.

The constant C in the ψ_1 function remains to be evaluated from some additional boundary condition. Reference 3 gives an expression for the tangential velocity profile in the core ($0 < r < r_n$) region, obtained by assuming $v(0) = 0$ and $\rho u r = (\rho u r)_o (r/r_n)^2$. The constant C in equation (11) is obtained by equating dv'/dr from equation (10) and dv'/dr' from the reference 3 profile at $r = r_n$. This gives:

$$C = \left(\frac{1}{2 - Re}\right)\left(\frac{Re}{C^{Re/2} - 1}\right) \tag{13}$$

Equation (13) is used throughout this report, and if combined with equations (10) and (11) gives the same tangential velocity profile as was obtained in reference 3. As $Re \rightarrow \infty$ (inviscid flow), $\psi_1 \rightarrow 1$, and equation (10) yields the ideal fluid relation of equation (8). This suggests that the function ψ_1 may be viewed as a "correction factor" which accounts for viscous effects on the ideal velocity profile.

Equations (1), (3), (4), and (5) can be combined, and the boundary condition $t(r \rightarrow \infty) = T_\infty$ applied to give the energy relation:

$$t = T_\infty - \frac{\frac{1}{2}\left(\frac{v_o r_o}{r}\right)^2 (\psi_2 - \psi_3)}{c_p g J} \tag{14}$$

where

$$\psi_2 = \left(\frac{1}{v_o' r_o'}\right)^2 \left[(1 - c)^2 + \frac{4}{Re} \frac{C - C^2}{(r')^{Re-2}} + \frac{1}{Re - 1} \frac{C^2}{(r')^{2Re-4}}\right] \quad (15)$$

$$\psi_3 = \left(\frac{1}{v_o' r_o'}\right)^2 \left[\frac{4}{Re}(1 - c)^2 + \frac{8}{Re} \frac{C - C^2}{(r')^{Re-2}} + \frac{Re}{Re - 1} \frac{C^2}{(r')^{2Re-4}}\right] \quad (16)$$

The function ψ_2 represents the effect of viscosity on radial momentum, and ψ_3 the effect of the viscous dissipation term, the right side of equation (3). As before, when $Re \to \infty$, $\psi_2 \to 1$, and $\psi_3 \to 0$, and equation (14) gives the isentropic relation. Equation (14), then, gives the variation of static temperature with radius. The total-temperature variation is given by:

$$T = t + \frac{v^2}{2c_p g J} \quad (17)$$

where v is given as a function of radius by equation (10).

By utilizing assumption (6), equations (1) and (5) can be combined to give the static-pressure gradient as:

$$\frac{1}{(p/p_o)} \frac{d(p/p_o)}{dr'} = \frac{Mv^2}{gRtr'} \quad (18)$$

Equation (18) is nonlinear and was solved by the Runge-Kutta numerical method on an IBM 704 computer. The boundary condition for equation (18) is $p/p_o = 1$ at $r' = r_o'$. The total pressure is given by equation (6).

All the working equations necessary to define the fluid dynamics of the system (eqs. (10) to (18)) as written are for laminar flow. That is, Re is given by Re_l as defined by equation (12). These equations were used for turbulent flow by virtue of assumption (8), that turbulent flow can be represented by laminar relations if μ is replaced by $\rho\epsilon$:

$$Re_t = Re_l \frac{\mu}{\mu + \rho\epsilon} \simeq Re_l \frac{\mu}{\rho\epsilon} \quad (19)$$

All equations remain as given, and the Reynolds number is now:

$$Re = Re_t \equiv \frac{-\rho u r}{\rho\epsilon} = \frac{-u r}{\epsilon} \quad (20)$$

Mixing-Length Functions for Vortex Flow

In rectilinear flow, the viscous shear stress between two adjacent fluid particles due to a velocity gradient between them is given by:

$$\tau = \mu \frac{du}{dy} \qquad (21)$$

To account for the additional friction losses due to turbulent motion, Prandtl proposed a model based on a mixing length, or the average transverse distance a fluid particle travels before adjusting to local conditions. The assumptions that the velocity fluctuations normal and parallel to the flow are equal gave the total shear stress on the fluid as:

$$\tau = (\mu + E_m) \frac{du}{dy} \qquad (22)$$

where the eddy viscosity is defined as:

$$E_m \equiv \rho l^2 \frac{du}{dy} \qquad (23)$$

A more detailed discussion of this development may be found in reference 14, pages 113 to 114, and reference 15.

Prandtl functions. - Reference 12 shows that the "shear velocity" (du/dy in pipe flow) in circular flow is given by $\left(\frac{dv}{dr} - \frac{v}{r}\right)$ and suggests the possible assumption that the turbulent shear stress is proportional to $\rho l^2 \left(\frac{dv}{dr} - \frac{v}{r}\right)^2$. For pipe flow, Prandtl assumed that the mixing length was proportional to y, the distance from the wall. A similar assumption for vortex flow is that the mixing length is proportional to some characteristic dimension, assumed to be the radius:

$$l = Kr \qquad (24)$$

The eddy diffusivity for vortex flow may be expressed as:

$$\epsilon \equiv \frac{E_m}{\rho} = -l^2 \left(\frac{dv}{dr} - \frac{v}{r}\right) \qquad (25)$$

This assumes equal radial and tangential velocity fluctuations. Combining equations (24) and (25) gives:

$$\epsilon = -K^2 r^2 \left(\frac{dv}{dr} - \frac{v}{r}\right) \qquad (26)$$

If this expression is used, equation (20) becomes:

$$\text{Re}_t = \frac{1}{\kappa^2} \frac{ur}{r^2\left(\dfrac{dv}{dr} - \dfrac{v}{r}\right)} \tag{27}$$

If the inertia factor ur and the shear stress factor, in the denominator, are evaluated at some radius, equation (27) can be used to determine the turbulent Reynolds number. It is not clear, however, where to evaluate either of these factors. Since the outer and inner radii r_o and r_n bound all possible choices, they were used to give the following forms of equation (27):

$$\text{Re}_t = \frac{1}{\kappa^2} \frac{\left(\dfrac{u_o}{v_o}\right)(v_o' v_o')}{r_o'^2\left(\dfrac{dv'}{dr'} - \dfrac{v'}{r'}\right)_o} \qquad \begin{array}{l}\text{Inertia at } r_o \\[6pt] \text{Shear stress at } r_o\end{array} \tag{27a}$$

$$\text{Re}_t = \frac{1}{\kappa^2} \frac{\left(\dfrac{u_o}{v_o}\right)(v_o' r_o')}{\left(\dfrac{dv'}{dr'} - \dfrac{v'}{r'}\right)_n} \qquad \begin{array}{l}\text{Inertia at } r_o \\[6pt] \text{Shear stress at } r_n\end{array} \tag{27b}$$

$$\text{Re}_t = \frac{1}{\kappa^2} \frac{\dfrac{u_n}{v_n}}{r_o'^2\left(\dfrac{dv'}{dr'} - \dfrac{v'}{r'}\right)_o} \qquad \begin{array}{l}\text{Inertia at } r_n \\[6pt] \text{Shear stress at } r_o\end{array} \tag{27c}$$

$$\text{Re}_t = \frac{1}{\kappa^2} \frac{\dfrac{u_n}{v_n}}{\left(\dfrac{dv'}{dr'} - \dfrac{v'}{r'}\right)_n} \qquad \begin{array}{l}\text{Inertia at } r_n \\[6pt] \text{Shear stress at } r_n\end{array} \tag{27d}$$

Kárman functions. - Instead of taking the mixing length proportional to a characteristic dimension as did Prandtl, von Kárman proposed a similarity hypothesis for turbulent motion (ref. 15, ch. 3). In a like manner, it is assumed that turbulence in vortex flow is influenced only by local conditions, represented by the shear stress and its derivatives, and that a similarity exists from point to point in the system such that the turbulence functions vary only by a scale factor, assumed to be the

12

mixing length. From this, the mixing length in a vortex is given by:

$$l = -\kappa \frac{\frac{dv}{dr} - \frac{v}{r}}{\frac{d}{dr}\left(\frac{dv}{dr} - \frac{v}{r}\right)}$$ (28)

This expression for mixing length gives the eddy diffusivity as:

$$\epsilon = -\kappa^2 \frac{\left(\frac{dv}{dr} - \frac{v}{r}\right)^3}{\left[\frac{d}{dr}\left(\frac{dv}{dr} - \frac{v}{r}\right)\right]^2}$$ (29)

This expression can also be obtained by dimensional analysis (ref. 3). Using this expression for eddy diffusivity in Reynolds number gives:

$$Re_t = \frac{1}{\kappa^2} \frac{ur\left[\frac{d}{dr}\left(\frac{dv}{dr} - \frac{v}{r}\right)\right]^2}{\left(\frac{dv}{dr} - \frac{v}{r}\right)^3}$$ (30)

As before, both the inertia factor and the shear stress factor can be evaluated at either r_o or r_n:

$$Re_t = \frac{1}{\kappa^2} \frac{\left(\frac{u_o}{v_o}\right)(v_o'r_o')\left[\frac{d}{dr'}\left(\frac{dv'}{dr'} - \frac{v'}{r'}\right)\right]_o^2}{\left(\frac{dv'}{dr'} - \frac{v'}{r'}\right)_o^3}$$ (30a)

$$Re_t = \frac{1}{\kappa^2} \frac{\left(\frac{u_o}{v_o}\right)(v_o'r_o')\left[\frac{d}{dr'}\left(\frac{dv'}{dr'} - \frac{v'}{r'}\right)\right]_o^2}{\left(\frac{dv'}{dr'} - \frac{v'}{r'}\right)_n^3}$$ (30b)

$$Re_t = \frac{1}{\kappa^2} \frac{\left(\frac{u_n}{v_n}\right)\left[\frac{d}{dr'}\left(\frac{dv'}{dr'} - \frac{v'}{r'}\right)\right]_o^2}{\left(\frac{dv'}{dr'} - \frac{v'}{r'}\right)_o^3}$$ (30c)

$$Re_t = \frac{1}{\kappa^2} \frac{\left(\frac{u_n}{v_n}\right)\left[\frac{d}{dr'}\left(\frac{dv'}{dr'} - \frac{v'}{r'}\right)\right]_n^2}{\left(\frac{dv'}{dr'} - \frac{v'}{r'}\right)_n^3} \tag{30d}$$

Modified Kármán function. - As will be seen later, when experimental data were used to evaluate the constant κ from equation (30b), a different approach suggested itself. What follows was not apparent a priori, but was developed to give a physical interpretation of a mathematical function.

In the development of the mixing length functions for circular flow, one significant difference between vortex and pipe flow was not considered. In pipe flow the mean flow vector is parallel to the wall. This is not so in vortex flow; there is a velocity component away from the wall. It is this radial velocity which gives the fluid its radial inertia.

If it is postulated that the radial inertia at the outer boundary (the injection point) and the shear stress and its derivatives at the inner radius are the determining factors of turbulence, then:

$$\epsilon = f\left[(ur)_o, \left(\frac{dv}{dr} - \frac{v}{r}\right)_n, \frac{d}{dr}\left(\frac{dv}{dr} - \frac{v}{r}\right)_n\right] \tag{31}$$

From dimensional analysis:

$$\epsilon = C_1(u_o r_o)^a \left\{ \frac{\left(\frac{dv}{dr} - \frac{v}{r}\right)_n^3}{\left[\frac{d}{dr}\left(\frac{dv}{dr} - \frac{v}{r}\right)\right]_n^2} \right\}^{1-a} \tag{32}$$

Equation (32) can be expressed in dimensionless form as:

$$Re_t = C_2 \left\{ \frac{\left(\frac{u_o}{v_o}\right)(v_o' r_o')\left[\frac{d}{dr'}\left(\frac{dv'}{dr'} - \frac{v'}{r'}\right)\right]_n^2}{\left(\frac{dv'}{dr'} - \frac{v'}{r'}\right)_n^3} \right\}^{1-a} \tag{33}$$

Simplified forms. - It was suggested in reference 3 that near the outer boundary the tangential velocity variation is closely represented by equation (8); that is, the tangential velocity varies inversely with

14

radius. By using this simplification, both the Prandtl (eq. (27)) and the Kármán (eq. (30)) functions can be written in the form:

$$Re_t = C_0\left(\frac{-u_o}{v_o}\right) \qquad (34)$$

If equation (27) is combined with equation (8), the expression for C_0 is $1/2\kappa^2$; if equation (30) is used, C_0 is given by $2/\kappa^2$. With the assumption that the tangential velocity varies inversely with radius at the inner radius, admittedly a less defensible simplification, the Prandtl and Kármán functions may be written:

$$Re_t = C_0\left(\frac{-u_n}{v_n}\right) \qquad (35)$$

Again, C_0 represents $1/2\kappa^2$ from the Prandtl form and $2/\kappa^2$ from the Kármán expression.

An interesting development is obtained by writing equation (34) in the following form:

$$Re_t = C_0\left(\frac{-u_o}{v_o}\right) = \frac{-(\rho u r)_o}{\rho\epsilon} \qquad (36)$$

Multiplying by $(2\rho\epsilon v_o/\mu u_o)$ gives:

$$\left(\frac{\rho v D}{\mu}\right)_o = 2C_0\left(\frac{\rho\epsilon}{\mu}\right) \qquad (37)$$

Equation (37) illustrates the point that vortex data can be correlated equally well in terms of a laminar, tangential Reynolds number evaluated at the outer boundary. The data of reference 10 are presented in this manner and are included later in this report for comparison.

EXPERIMENT

Vortex Generator

The vortex test apparatus is shown in figure 1(a). It was designed to provide (1) tangential velocities up to 500 feet per second and mass flows up to 0.1 pound per second and (2) measurements of total and static pressure. Dry air at 70° F was regulated to maintain atmospheric pressure

in the vortex header and was exited to an altitude exhaust system which was capable of a minimum pressure of 26 inches of mercury below atmospheric.

The test section was constructed from Lucite to permit visual observation. The radius of the vortex cavity was 6 inches; the axial length was 6 inches; and the exhaust-nozzle radius was 1.75 inches. The vortex flow was induced by 16 guide vanes which formed the cylindrical surface bounding the test cavity. The air was introduced through the 16 slits which ran the entire 6-inch axial length; the slit opening was 0.006 to 0.008 inch. The inner chord length of a guide vane was 2.4 inches. Figure 1(b) is a schematic drawing of the vortex generator.

Instrumentation

Static-pressure taps and total-pressure probes were located on both end faces of the vortex as shown in figure 1(a). The total-pressure probes were fabricated from 10-mil-outside-diameter tubing with a 3-mil wall thickness. During test runs the probe tips were alined to give maximum readings. A probe position normal to the radius gave maximum velocity readings in all cases.

Total-pressure readings were taken at two radial stations for each run; these were located at radii of 4.75 and 2.5 inches. No total-pressure readings were taken in the central core of the vortex $(r < r_n)$ because of difficulties arising from the fact that the probe tip would be in its own wake. Though not included in this report, measurements were taken at various probe depths to study any possible axial variation of tangential velocity. No such a dependence was indicated; all total-pressure data reported herein were obtained at a depth of 2.5 inches.

Data Reduction

Tangential velocities were calculated from the measured static and total pressures at the two stations $r_4 = 4.75$ inches and $r_{10} = 2.5$ inches. Equations (6) and (17) may be written in the form:

$$v = \left(\frac{2gJc_pTP^*}{1 + P^*}\right)^{1/2} \tag{38}$$

where

$$P^* \equiv \left(\frac{P}{p}\right)^{\frac{\gamma-1}{1}} - 1 \tag{39}$$

The total temperature T was taken as 530° R in all cases; an error of 10° F in T would cause a 1-percent error in velocity. An IBM 704 code was used to iteratively select the v_0 and Re_t from equation (10), which gave v_4 and v_{10} within 1/2 percent of the values computed from data using equation (38). This Re_t was then used with equation (18) to compute the variation of p/p_0 with radius, and this curve was compared with the data.

Figures 2(a) to (c) show the static-pressure and velocity variations for low, medium, and high vortex strengths, respectively. The static-pressure variation calculated from the analytical equations, using the turbulent Reynolds number indicated by the tangential velocities, is in good agreement with the experimental data. For comparison, the curves for inviscid flow, computed from equations (6), (7), and (8), are also shown.

The remaining parameters needed to evaluate the various mixing length functions were computed from:

$$u_0 = \frac{-w}{2\pi L r_0 \rho_0} \qquad (40)$$

$$u_n = \frac{-w}{2\pi L r_n \rho_n} \qquad (41)$$

$$v_n = \frac{v_0 r_0}{r_n} \sqrt{\psi_{1,n}} \qquad (42)$$

The derivatives dv/dr and d^2v/dr^2 were evaluated from equation (10).

RESULTS AND DISCUSSION

In figures 3, 5, and 6 various data symbols are used to denote two series of runs; in figures 4 and 7 the data of both series are noted by the same symbol. Each series represents a range of mass-flow rates from the lowest measurable to the highest possible. After the first set of data, noted by round symbols, was completed, the test section was completely dissembled. Then, with no particular emphasis on duplicate blade settings, the generator was reassembled, and the data indicated by the square symbols were obtained. All the experimental data of this investigation are listed in table I.

During both series of runs, a phenomenon was observed which was felt to warrant identification in figures 3, 5, and 6. At low vortex

E-1145

strengths, the noise associated with the airflow was essentially silent. As the vortex strength was increased, a point was reached - corresponding to a tangential velocity of about 300 feet per second - at which a monotone "whistle" was emitted from the test section. Subsequent measurements proved this tone to be essentially a pure one, with a frequency of approximately 1200 cycles per second. The whistle persisted with increasing vortex strength up to a tangential velocity of 400 feet per second. At this point the sound increased, essentially as a step function, to a much louder, discordant sound more properly labeled "scream". This scream was found to be comprised of many overtones and harmonics and of other 1200-cycle sounds out of phase with each other.

It was felt that these high-frequency waves in the vortex cavity might well affect the turbulence level of the flow. The plain symbols represent silent operation; tailed symbols represent whistle runs; and the symbols for the scream runs are solid. Some of the data do show a clearly ordered relation with respect to the three regimes of operation; for this reason, such identification has been maintained although the cause of the sounds is not fully understood.

Simplified Functions

Turbulent Reynolds numbers and radial-to-tangential velocity ratios were computed from the experimental data. Figure 3(a) shows the results of evaluating the velocity ratio at the outer boundary of the vortex. Each data point represents an experimental run, for which a turbulent Reynolds number and v_O were determined from equation (10) and measured values of v_4 and v_{10}. The value of u_O was computed from equation (40) and a measured weight flow rate. The line through the data was drawn so as to go through the origin $\left(\text{Re}_t = 0, -\dfrac{u_O}{v_O} = 0\right)$, since no intercept is permitted by the form of equation (34). Though considerable scatter is present, the data are reasonably well represented by the line.

The value of the universal constant κ was computed from the slope to be 0.038, using $C_O = 1/2\kappa^2$. This is not in agreement with the value of 0.4 that has been well established for pipe flow. A possible explanation is that the universal constant is perhaps more constant than universal; that is, it has one constant value for vortex flow, and another constant value for rectilinear flow. Such a conclusion is only suggested by the few data of figure 3(a), however, and further evaluation would require additional independent studies.

Figure 3(b) was obtained by evaluating the velocity ratio at the inner boundary r_n. The extreme scatter of the data reflects the inadequacy of the assumption that the tangential velocity varies inversely with the radius in the vicinity of r_n. Again, the "best" line intersects the origin and gives a value of κ of 0.063 for $C_O = 1/2\kappa^2$. The dashed line represents a κ of 0.038, shown for comparison.

The indication of figure 3 is that the assumption of an ideal flow variation of tangential velocity with radius at the outer boundary of a vortex is a reasonable one. If a value $\kappa = 0.038$ is used, the turbulent Reynolds number can be obtained from equation (34) with $C_0 = 1/2\kappa^2$.

As a part of a study of vortex flow in a gaseous reactor, turbulence data were obtained in reference 10 using vortex tubes that were 0.6, 1.0, and 2 inches in diameter with nitrogen and helium as fluids. By computing tangential velocities from measured static-pressure gradients and using essentially the same technique as described herein to obtain turbulent Reynolds numbers, the eddy-to-laminar viscosity ratio $\rho\epsilon/\mu$ was correlated with a laminar, tangential Reynolds number evaluated at the periphery $(\rho v D/\mu)_0$. These data and the data of this investigation are shown in figure 4.

The slope of the line through the data of this report was taken to be 1.0, as suggested by the form of equation (37). The degree of correlation in figure 4 is exactly the same as that shown in figure 3(a), since equation (37) is simply an algebraic restatement of equation (34). The line with a slope of 0.86 is a least-mean-squares fit obtained in reference 10. The line with a slope of 1.0 was drawn to permit a comparison and gave a value of κ from the data of reference 10 of 0.02, as compared with the 0.038 obtained from the data of this report.

This again suggests the possibility that the coefficient κ is a function of the flow pattern and, since all the data of figure 4 are from vortices, fluid or geometry parameters as well. Any such conclusion, however, is predicated on the validity of the two assumptions of constant $(\rho\epsilon)$ with radius and of equal radial and tangential velocity fluctuations. The former assumption is estimated to be the more doubtful.

Prandtl Functions

Figures 5(a) to (d) show the data evaluated in the form of Prandtl functions given by equations (27a) to (27d), respectively. In both figures 5 and 6, all lines with a positive slope intersect the origin.

Figure 5(a) shows the data plotted in the form of equation (27a). Both the inertia factor and the shear stress factor are evaluated at the outer boundary r_0. Figure 5(a) shows essentially no cause-effect relation between ordinate and abscissa. The "best" line is shown only to permit a comparison of κ, or slope, from this plot with the other κ values.

Figure 5(b) shows a plot of equation (27b), with the inertia factor evaluated at r_0 and the shear stress at r_n. Although the data can be

represented by a straight line, a real value for κ cannot be obtained because the negative slope is not compatible with the form of equation (27b). No effect of noise level is apparent in figure 5(b).

Figure 5(c) shows the data plotted in the form of equation (27c), with the inertia factor evaluated at r_n and the shear stress at r_o. Although a trend with respect to noise level can be seen, any interpretation of figure 5(c) is questionable because of the excessive scatter. The line shown goes through the origin and gives $\kappa = 0.05$.

The data shown in figure 5(d) are plotted in the form of equation (27d), with both the inertia and shear stress factors evaluated at r_n. As in figure 5(b), the slope is negative, and there is no real value of κ in equation (27d). While considerable scatter is present, the apparent trend in the data with respect to noise seemed to warrant identification. Three lines are shown in figure 5(d) denoting silent, whistle, or scream as the characteristic sound of operation. An investigation of the cause and nature of these sounds was beyond the scope of this study, but figure 5(d) indicates that they are related to turbulence effects in the vortex.

To sum up, the only Prandtl function which correlated the experimental data was the one obtained by evaluating the inertia factor at the outer boundary and the shear stress at the inner boundary. However, the slope of the straight line through the data was negative; this is not in accord with the form of the equation which was used to relate the dependent and independent variables.

Kármán Functions

Figures 6(a) to (d) show the data evaluated in the form of Kármán functions given by equations (30a) to (30d), respectively. Again, all lines with a positive slope intersect the origin.

Figure 6(a) shows the result of evaluating both the inertia factor and the shear stress at the outer boundary. This corresponds to the Prandtl function of figure 5(a). The Kármán function represents the data reasonably well and gives a value of $\kappa = 0.063$. The parameters plotted are those given by equation (30a).

The Kármán function given in equation (30b), with the inertia factor evaluated at r_o and the shear stress at r_n, is shown in figure 6(b). Here the data are seen to exhibit very little scatter. These boundary conditions also gave the best correlation with the Prandtl function (fig. 5(b)). A straight line through the data (shown dashed) has a negative slope, which does not admit of a real root for the κ^2 in equation (30b).

The line from figure 5(b) is shown for comparison. The "best" line through the data (shown solid) has a slight curvature. It was this that first suggested a log-log plot, and the possibility of an exponential dependency of the variables.

Figure 6(c) shows the result of evaluating the inertia factor at r_n and the shear stress at r_o. The scatter of the data is excessive, as was the case with the corresponding Prandtl function in figure 5(c). The parameters plotted are given by equation (30c).

Figure 6(d) was obtained from equation (30d), with both the inertia factor and the shear stress evaluated at r_n. The use of these boundary conditions results in a separation of the data with respect to the sound characteristic of operation. This trend was also exhibited by the Prandtl function with these boundary conditions (fig. 5(d)).

The Kármán functions correlate the experimental data better than do corresponding Prandtl functions for the same boundary conditions. The best agreement is obtained by evaluating the inertia factor at the outer boundary and the shear stress at the inner one. For these boundary conditions, the experimental data exhibit a negative slope; this is incompatible with the form of both the Prandtl and Kármán relations. This indicates that the ordinate and abscissa variables do have a functional relation, but that the model which resulted in equation (28) is incomplete.

Modified Kármán Function

The trend of the data shown in figure 6(b) suggested an exponential variation. Figure 7 is a replot of figure 6(b) on log-log coordinates. A log-log plot of the corresponding Prandtl function (fig. 5(b)) would have a similar appearance, but was not used because less scatter was exhibited in figure 6(b). All the data are shown; no identification is made of either the noise characteristic or the run sequence. The data are represented by a straight line with very little scatter. The constants in equation (33) were determined from figure 7 to be:

$$a = 1.2$$

$$C_2 = 0.815$$

The experimental data are best correlated, then, by the modified
Kármán function:

$$Re_t = C_2 \left\{ \frac{\left(\frac{u_o}{v_o}\right)(v'_o r'_o)\left[\frac{d}{dr'}\left(\frac{dv'}{dr'} - \frac{v'}{r'}\right)\right]_n^2}{\left(\frac{dv'}{dr'} - \frac{v'}{r'}\right)_n^3} \right\}^{1-a} \tag{33}$$

While it is probable that the constants C_2 and a are functions of the
system geometry and perhaps fluid properties, it is felt that equation
(33) does indicate the functional relation of shear stress, inertia, and
eddy diffusivity in a turbulent vortex. Subject to the validity of the
two primary assumptions - that $\rho\epsilon$ is constant with radius and that
radial and tangential velocity fluctuations are equal - the data indicate
that eddy diffusivity in a turbulent vortex is a function of both radial
inertia and shear stress derivatives.

SUMMARY OF RESULTS

A series of runs were made with a vortex generator, using air as the
fluid. Static pressures were measured at various radial stations; two
total pressures were measured. A turbulent Reynolds number was determined
for each run by matching the experimental velocities to a closed-form so-
lution of the Navier-Stokes equations of motion for compressible flow in
the annular region of a vortex; the eddy viscosity is assumed to be con-
stant with radius. An expression for eddy diffusivity is developed for
vortex flow in terms of a Prandtl mixing length and a shear velocity.

Prandtl mixing length functions are obtained for vortex flow with
the assumption that mixing length is proportional to radius. Kármán
functions are developed by applying a similarity hypothesis to vortex
flow; the scale factor is taken to be the mixing length. The Prandtl and
Kármán functions contain an inertia factor and a shear stress factor. The
experimental data and the Navier-Stokes solutions are used to evaluate
these factors at inner and outer boundaries of the vortex. The following
results were obtained:

1. Some combinations of the assumed boundary conditions gave functions
which either did not correlate the experimental data or gave imaginary
values of the universal constant κ.

2. Kármán mixing length functions correlate the data better than
Prandtl ones for similar boundary conditions.

3. The universal constant κ was found to be 0.04 to 0.08 for vortex flow, rather than the 0.4 established for pipe flow.

4. The Kármán expression evaluated by defining both the inertia and he shear stress at the outer boundary correlates the data without excessive scatter for $\kappa = 0.063$.

5. The data are best correlated by a modified Kármán expression which is developed by dimensional analysis. It is assumed that, in addition to the shear stress and its derivatives, the eddy diffusivity is a function of the radial fluid momentum at the outer vortex boundary.

Lewis Research Center
  National Aeronautics and Space Administration
    Cleveland, Ohio, June 12, 1961

REFERENCES

1. Hartnett, J. P., and Eckert, E. R. G.: Experimental Study of the Velocity and Temperature Distribution in a High-Velocity Vortex-Type Flow. Trans. ASME, vol. 79, no. 4, May 1957, pp. 751-758.

2. Savino, J. M., and Ragsdale, R. G.: Some Temperature and Pressure Measurements in Confined Vortex Fields. Preprint 60-SA-4, ASME, 1960.

3. Deissler, R. G., and Perlmutter, M.: Analysis of the Flow and Energy Separation in a Turbulent Vortex. Int. Jour. Heat and Mass Transfer, vol. 1, no. 2, Pergamon Press, 1960.

4. Rott, Nicholas: On the Viscous Core of a Line Vortex. ZAMP, vol. lXb, fasc. 5/6, 1958, pp. 543-553.

5. Mack, L. M.: The Compressible, Viscous, Heat-Conducting Vortex. Prog. Rep. 20-328, Jet Prop. Lab., C.I.T., May 1, 1959.

6. Marxman, G. A., and Kerrebrock, J. L.: Heat Transfer in a Two-Dimensional Vortex Flow of a Dissociating Gas. STL/TR 60-000-09061, Prop. Lab., Space Tech. Labs., Inc., Feb. 26, 1960.

7. Lewellen, W. S.: Magnetohydrodynamically Driven Vortices. Proc. Heat Transfer and Fluid Mech. Inst., 1960.

8. Bussard, R. W., and DeLauer, R. D.: Nuclear Rocket Propulsion. McGraw-Hill Book Co., Inc., 1958, pp. 323-324.

9. Ragsdale, Robert G.: NASA Research on the Hydrodynamics of the Gaseous Vortex Reactor. NASA TN D-288, 1960.

10. Keyes, J. J., Jr., and Dial, R. E.: An Experimental Study of Vortex Flow for Application to Gas-Phase Fission Heating. ORNL 2837, Oak Ridge Nat. Lab., Apr. 16, 1960.

11. Rosenzweig, Martin L., Lewellen, W. S., and Kerrebrock, Jack L.: The Feasibility of Turbulent Vortex Containment in the Gaseous Fission Rocket. Preprint 1516A-60, Am. Rocket Soc., Inc., 1960.

12. Kassner, Rudolph, and Knoernschild, Eugen: Friction Laws and Energy Transfer in Circular Flow. Tech. Rep. F-TR-2198-ND, Air Materiel Command, Wright-Patterson Air Force Base, Mar. 1948.

13. Pai, Shih-I: Viscous Flow Theory. I - Laminar Flow. Ch. 3, D. Van Nostrand Co., Inc., 1956, p. 38.

14. Knudsen, James G., and Katz, Donald L.: Fluid Dynamics and Heat Transfer. McGraw-Hill Book Co., Inc., 1958, pp. 155-156.

15. Bakhmeteff, Boris A.: The Mechanics of Turbulent Flow. Princeton Univ. Press, 1941.

E-1145

TABLE I. - EXPERIMENTAL DATA

$$\left[r_0 = 6.0", \quad r_4 = 4.75", \quad r_{10} = 2.5", \quad r_n = 1.75", \quad T_0 = 530^\circ \text{ R.} \right]$$

| Run number	Airflow, w, lb/sec	Static pressure, in. Hg abs					Total pressure, in. Hg abs		Noise level
		p_0	p_4	p_{10}	p_n	$p_{r=0}$	p_4	p_{10}	
118	0.099	26.02	25.97	25.34	24.77	23.52	26.42	26.02	Silent
119	.1065	21.65	21.42	20.56	19.72	17.92	22.07	21.52	
120	.120	24.01	23.92	22.87	21.92	19.82	24.62	23.92	
121	.1185	22.82	22.62	21.80	21.12	19.82	23.22	22.62	
122	.128	21.02	20.72	19.49	18.12	15.57	21.62	20.82	
123	.1395	19.35	19.07	17.39	15.87	12.42	20.17	19.22	
124	.1485	19.65	19.32	17.53	15.82	12.02	20.57	19.52	
125	.1335	21.42	21.12	19.83	18.52	15.87	22.02	21.32	
126	.1545	18.57	18.12	16.06	14.07	9.87	19.52	18.27	Whistle
127	.163	18.70	18.32	16.10	13.92	9.32	19.77	18.42	Whistle
128	.1675	18.13	17.67	15.17	12.97	7.87	19.32	17.92	Silent
129	.1675	15.60	15.17	12.39	10.42	6.32	17.17	15.32	Scream
130	.172	15.10	14.72	11.77	9.82	5.57	16.92	14.87	
131	.180	15.35	14.77	11.89	9.72	5.32	17.07	14.92	
132	.163	14.63	14.22	11.51	9.57	5.52	16.32	14.37	
133	.153	14.60	14.27	11.77	9.97	6.17	16.17	14.37	
148	0.125	25.67	25.52	24.24	23.17	20.67	26.22	25.62	Silent
150	.121	18.48	18.32	17.11	15.92	13.27	19.02	18.37	
151	.131	19.87	19.72	18.29	17.07	14.22	20.47	19.82	
152	.139	21.39	21.17	19.63	18.32	15.17	22.07	21.27	
153	.144	23.75	23.47	21.88	20.27	16.72	24.47	23.67	
154	.143	21.69	21.42	19.65	17.97	14.17	22.47	21.62	
155	.1535	21.00	20.72	18.72	16.82	12.47	21.87	20.92	
156	.1555	19.20	18.92	16.80	14.82	10.32	20.12	19.02	Whistle
157	.166	19.67	19.27	16.90	14.82	8.72	20.67	19.47	
158	.170	19.73	19.32	16.87	14.62	9.22	20.82	19.62	
158-2	.178	20.13	19.67	16.90	14.37	8.27	21.32	19.97	
159	.186	20.07	19.57	16.60	13.87	7.42	21.37	19.97	
160	.185	19.32	18.82	15.28	12.82	7.32	21.02	19.12	Scream
161	.184	18.30	17.82	14.27	11.82	6.52	20.02	17.97	
162	.1895	18.33	17.67	14.03	11.57	6.12	20.12	17.82	
163	.1945	18.47	17.87	14.17	11.67	6.17	20.27	17.97	
164	.2065	19.13	18.52	14.68	12.12	6.32	21.02	18.72	
165	.239	20.43	19.72	15.62	12.82	7.42	22.42	19.92	
166	.2615	21.10	20.32	15.98	13.22	6.67	23.12	20.52	
167	.294	22.62	21.82	17.25	14.12	7.12	24.82	22.02	
168	.114	25.35	25.27	24.37	23.57	21.62	25.77	25.32	Silent
169	.102	25.76	25.67	24.91	24.27	22.72	26.17	25.72	Silent
170	.0865	24.73	24.62	23.98	23.42	22.12	24.92	24.62	
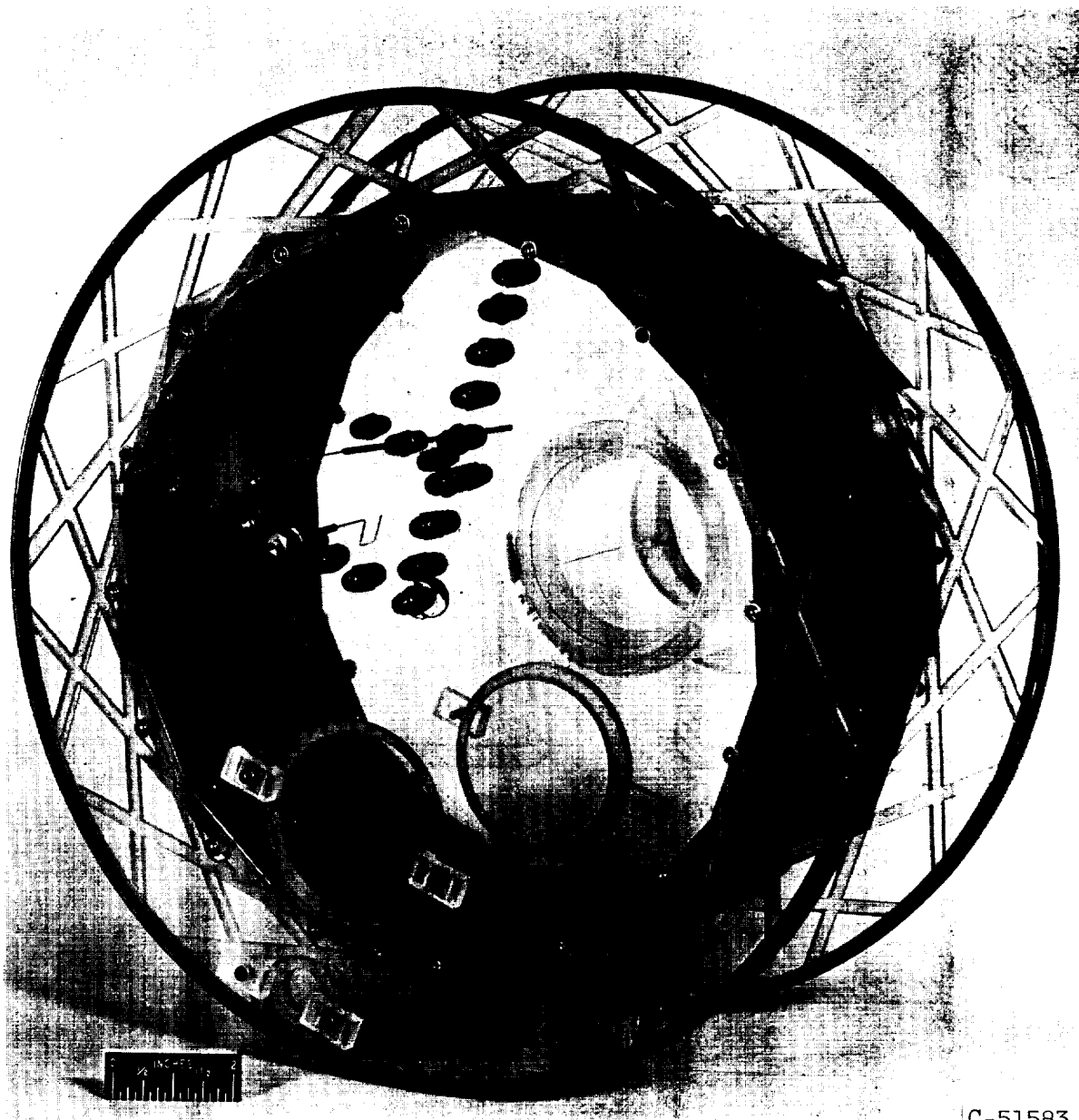
C-51583

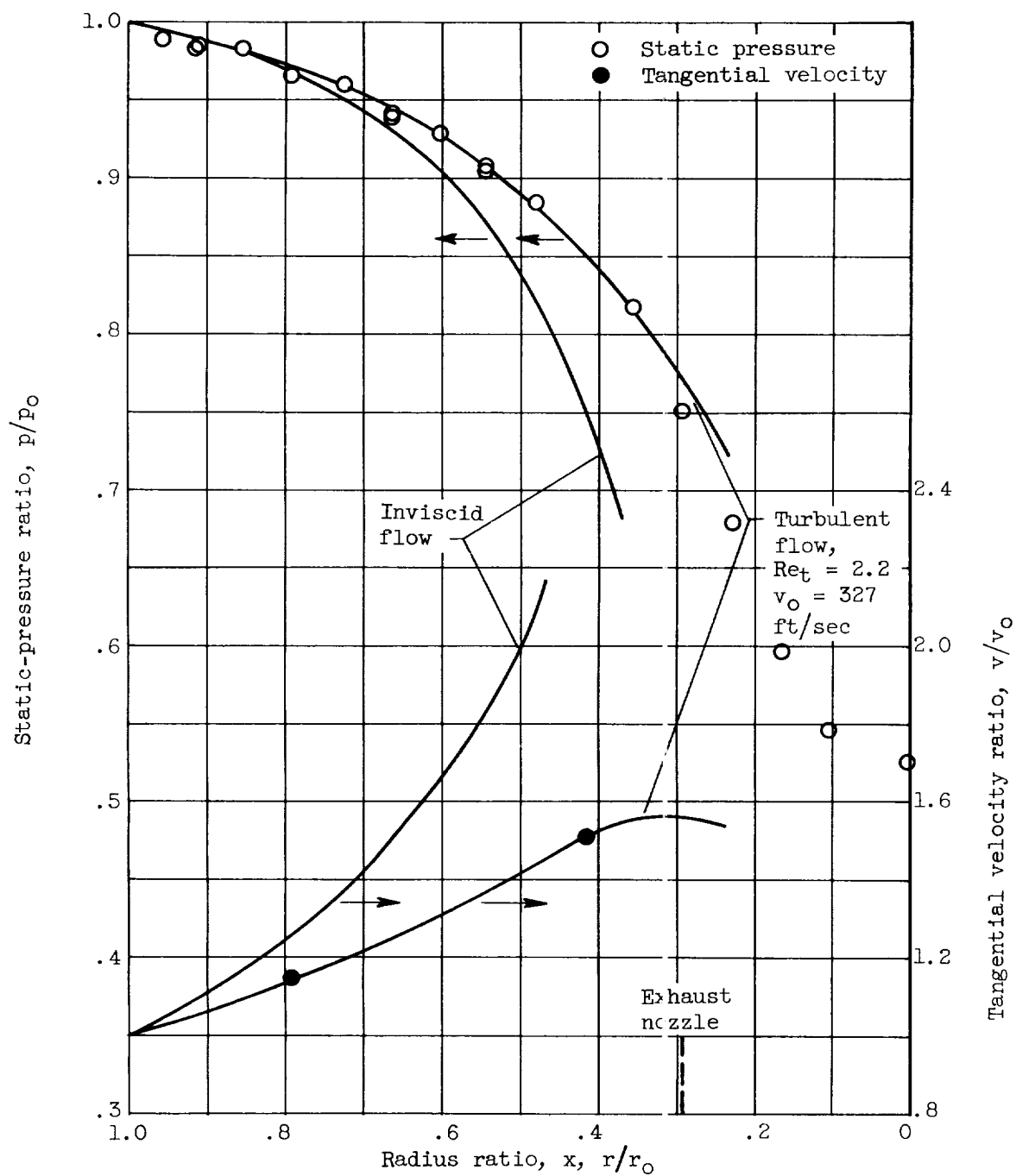(a) Photograph.

Figure 1. - Vortex test section.
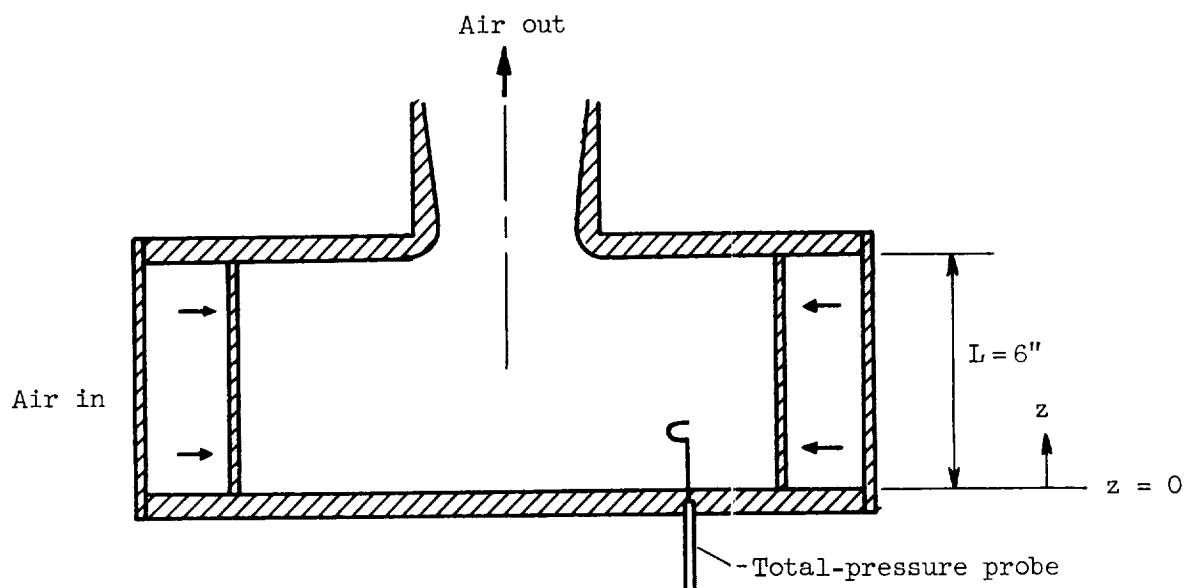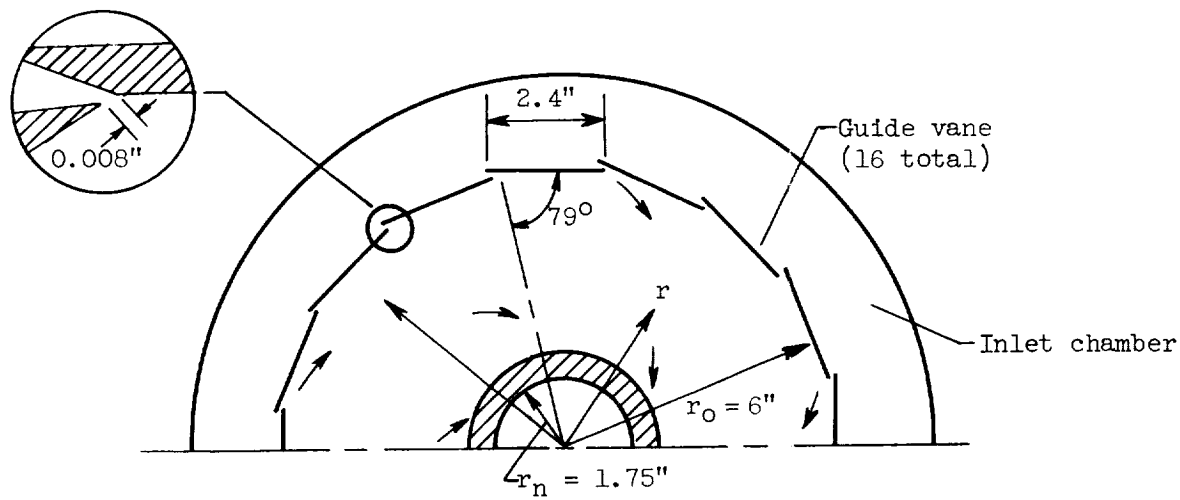
(b) Schematic diagram.

Figure 1. - Concluded. Vortex test section.
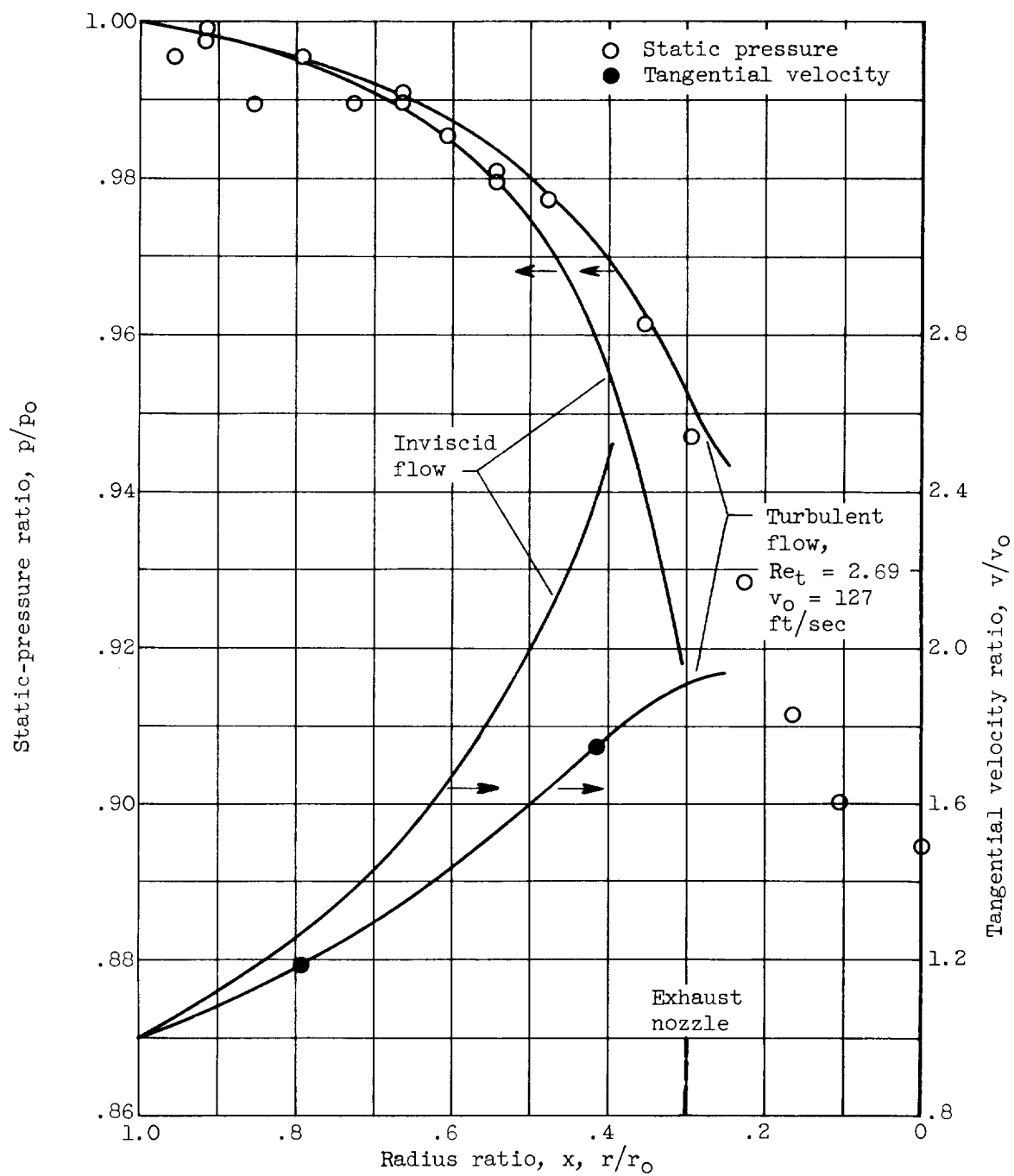
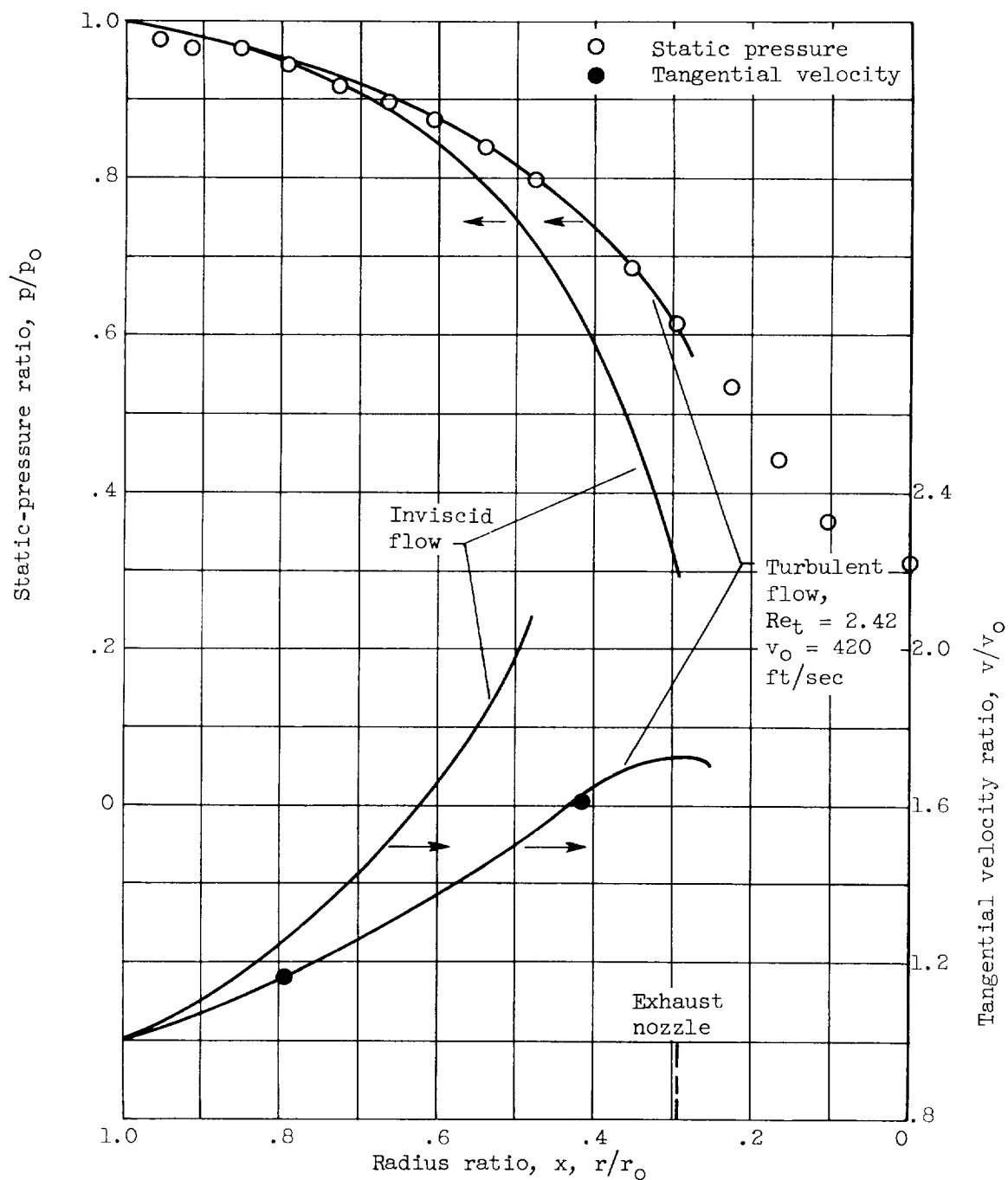E-1145

(a) Low vortex strength.

Figure 2. - Vortex static-pressure and tangential velocity data.

(b) Medium vortex strength.

Figure 2. - Continued. Vortex static-pressure and tangential velocity data.

(c) High vortex strength.

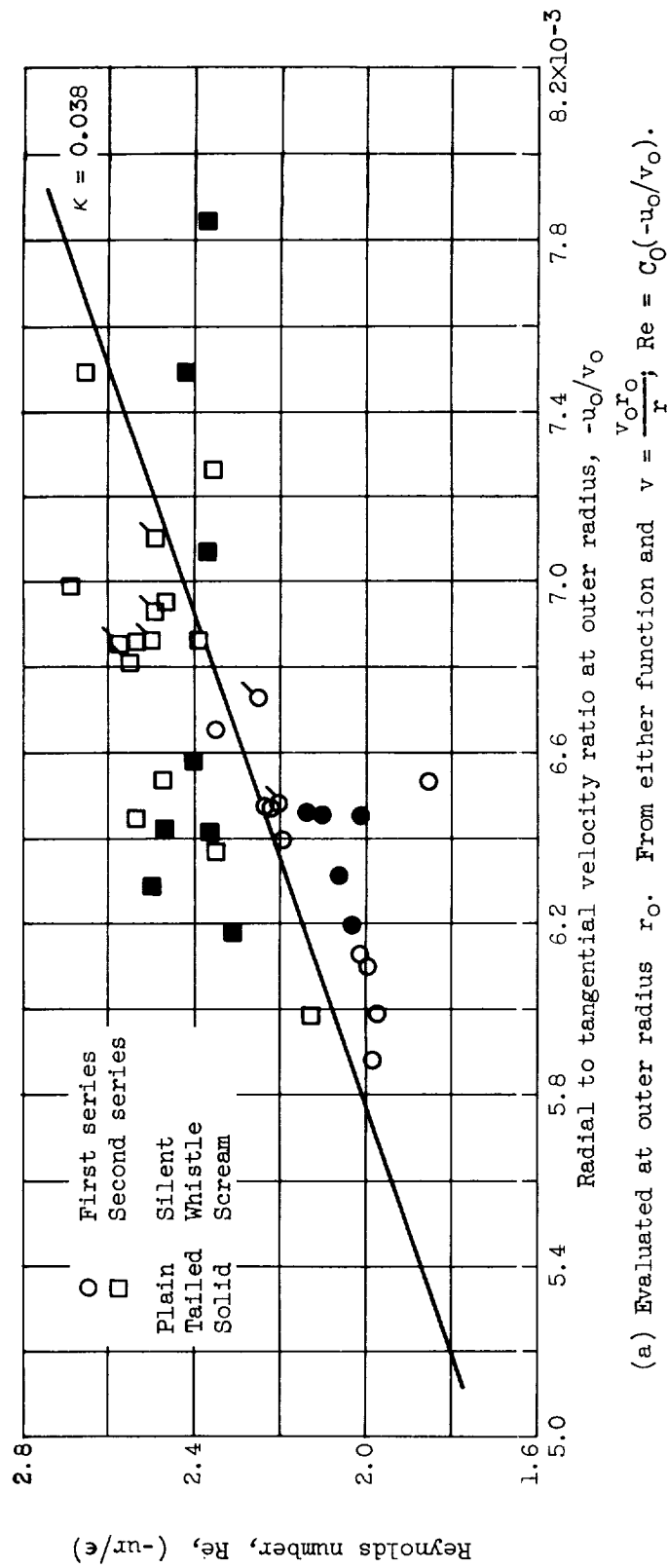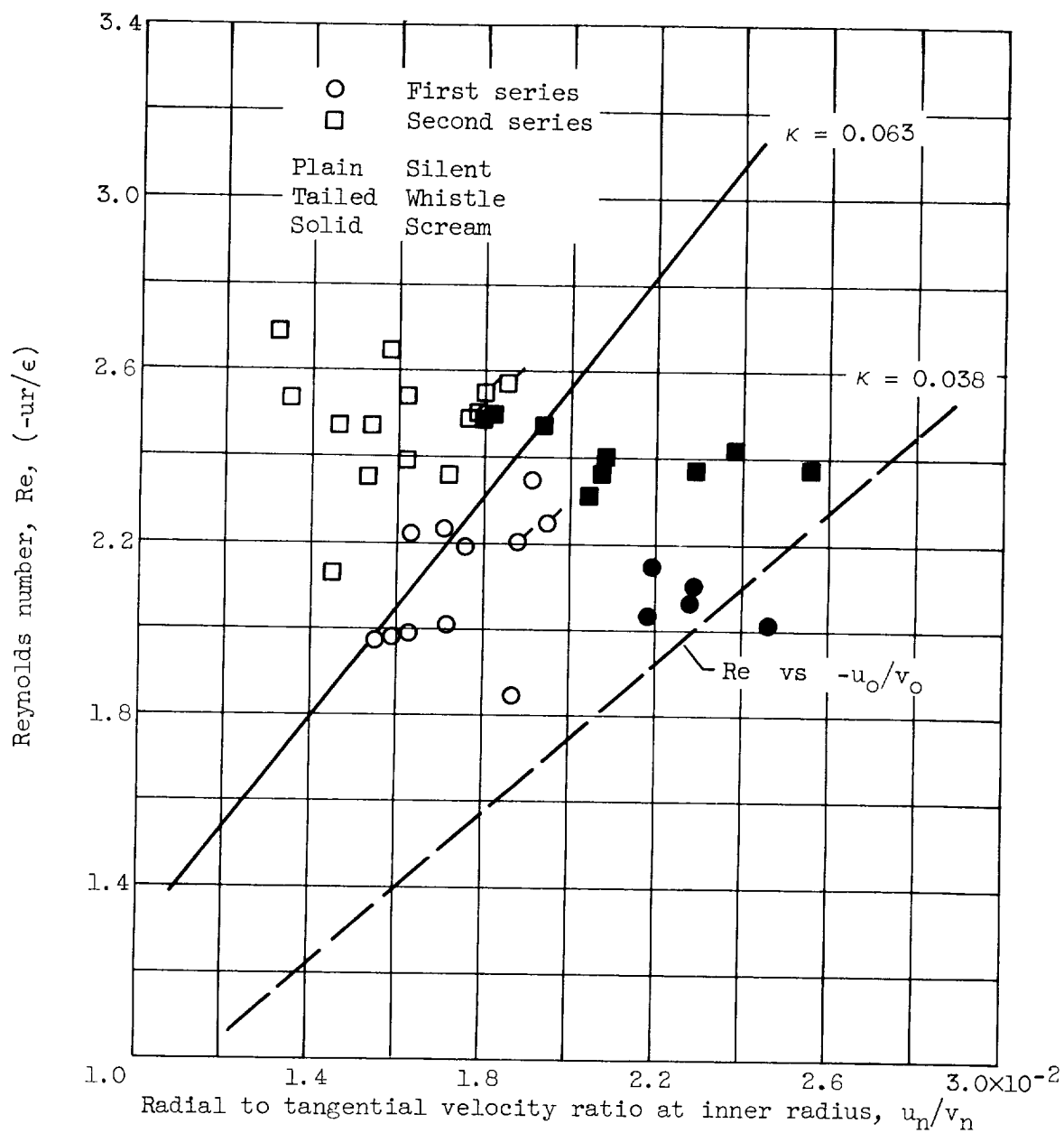Figure 2. - Concluded. Vortex static-pressure and tangential
velocity data.

(a) Evaluated at outer radius r_o. From either function and $v = \dfrac{v_o r_o}{r}$; $Re = C_0(-u_o/v_o)$.

Figure 3. - Simplified Kármán or Prandtl function.

E-1145

(b) Evaluated at inner radius r_n. From either function and

$$v = \frac{v_n r_n}{r}; \quad Re = C_0(-u_n/v_n).$$

Figure 3. - Concluded. Simplified Kármán or Prandtl function.
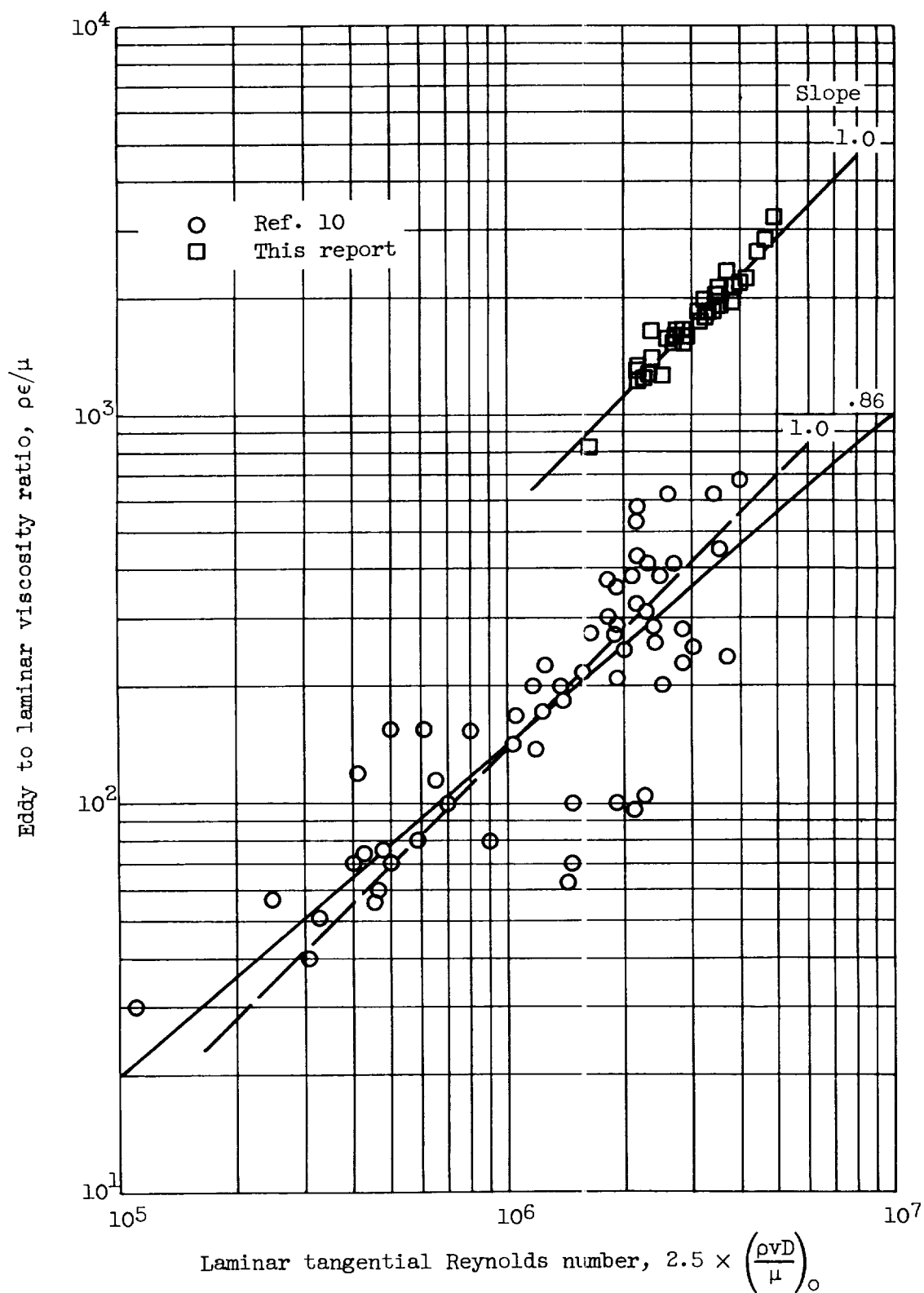
Figure 4. - Correlation of viscosity ratio with tangential
Reynolds number.
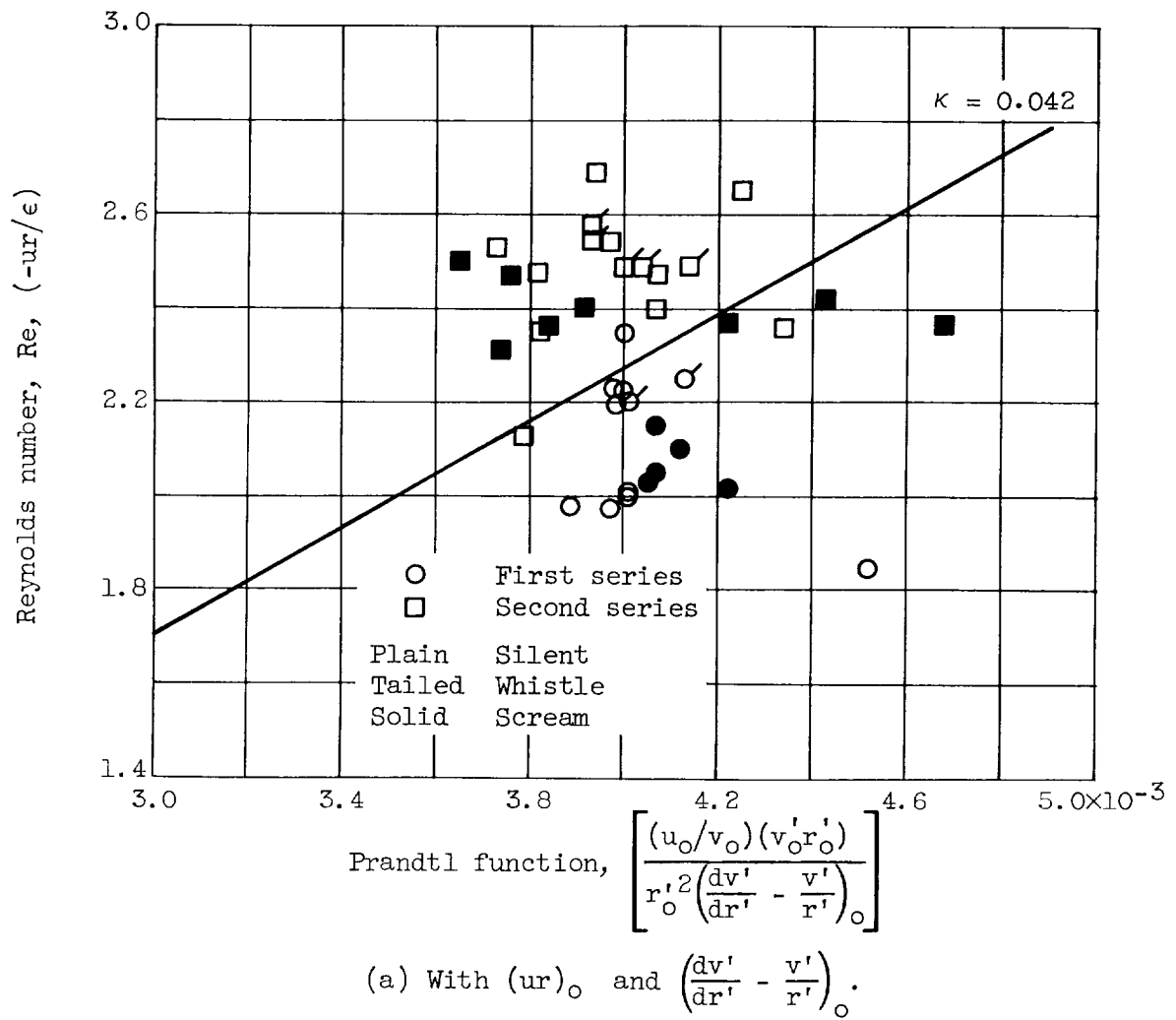
Figure 5. - Prandtl function.

(b) With $(ur)_0$ and $\left(\dfrac{dv'}{dr'} - \dfrac{v'}{r'}\right)_n$.

Figure 5. - Continued. Prandtl function.

E-1145

Reynolds number, Re, $(-ur/\epsilon)$

$\kappa = 0.05$

3.0

2.6

2.2

1.8

1.4

1.0

O   First series
□   Second series
Plain   Silent
Tailed   Whistle
Solid   Scream

2   3   4   5   6   7 8×10^{-3}

Prandtl function, $\left[\dfrac{u_n/v_n}{r_o'^2 \left(\dfrac{dv'}{dr'} - \dfrac{v'}{r'} \right)_o} \right]$

(c) With $(ur)_n$ and $\left(\dfrac{dv'}{dr'} - \dfrac{v'}{r'} \right)_o$.
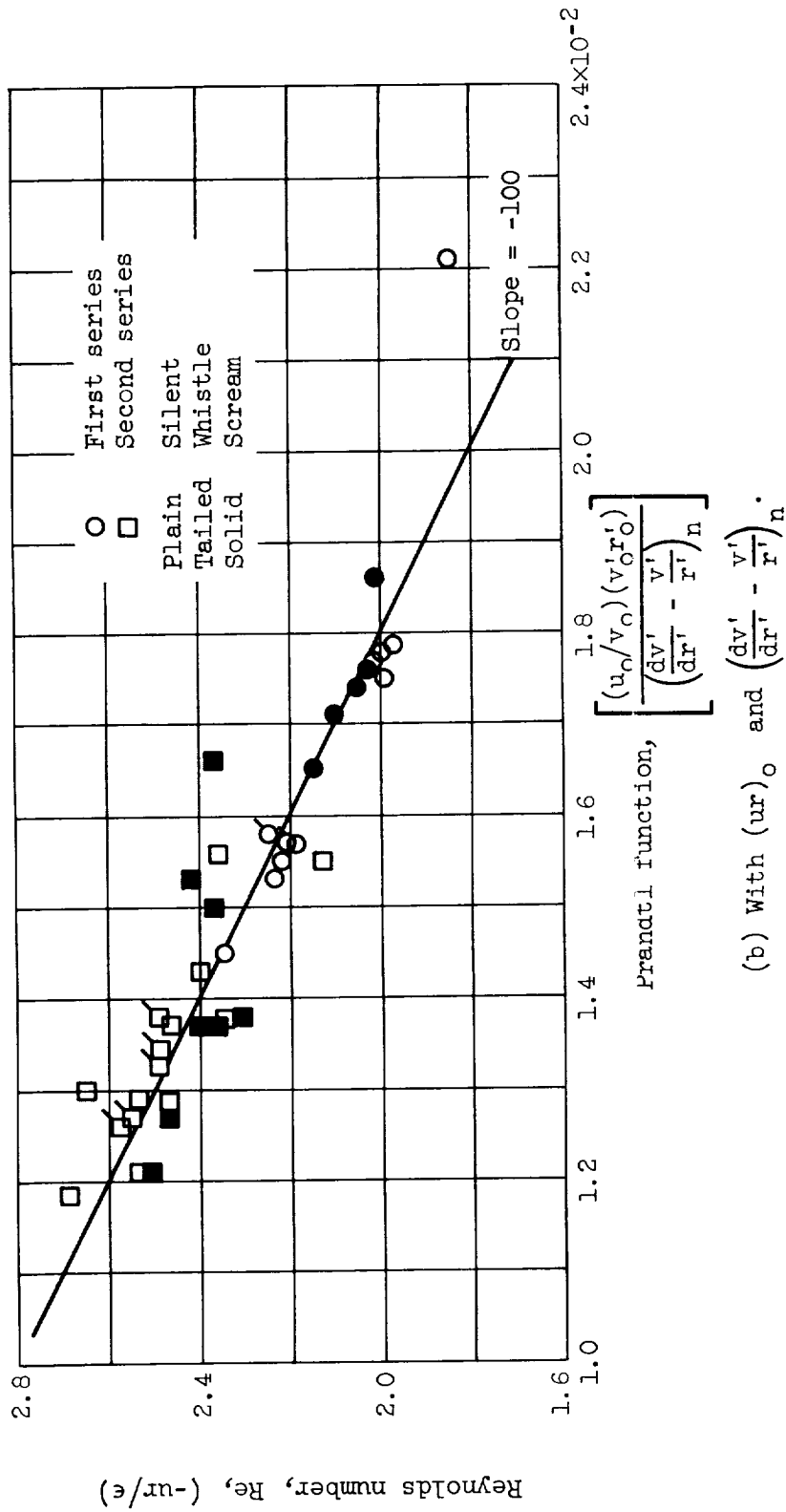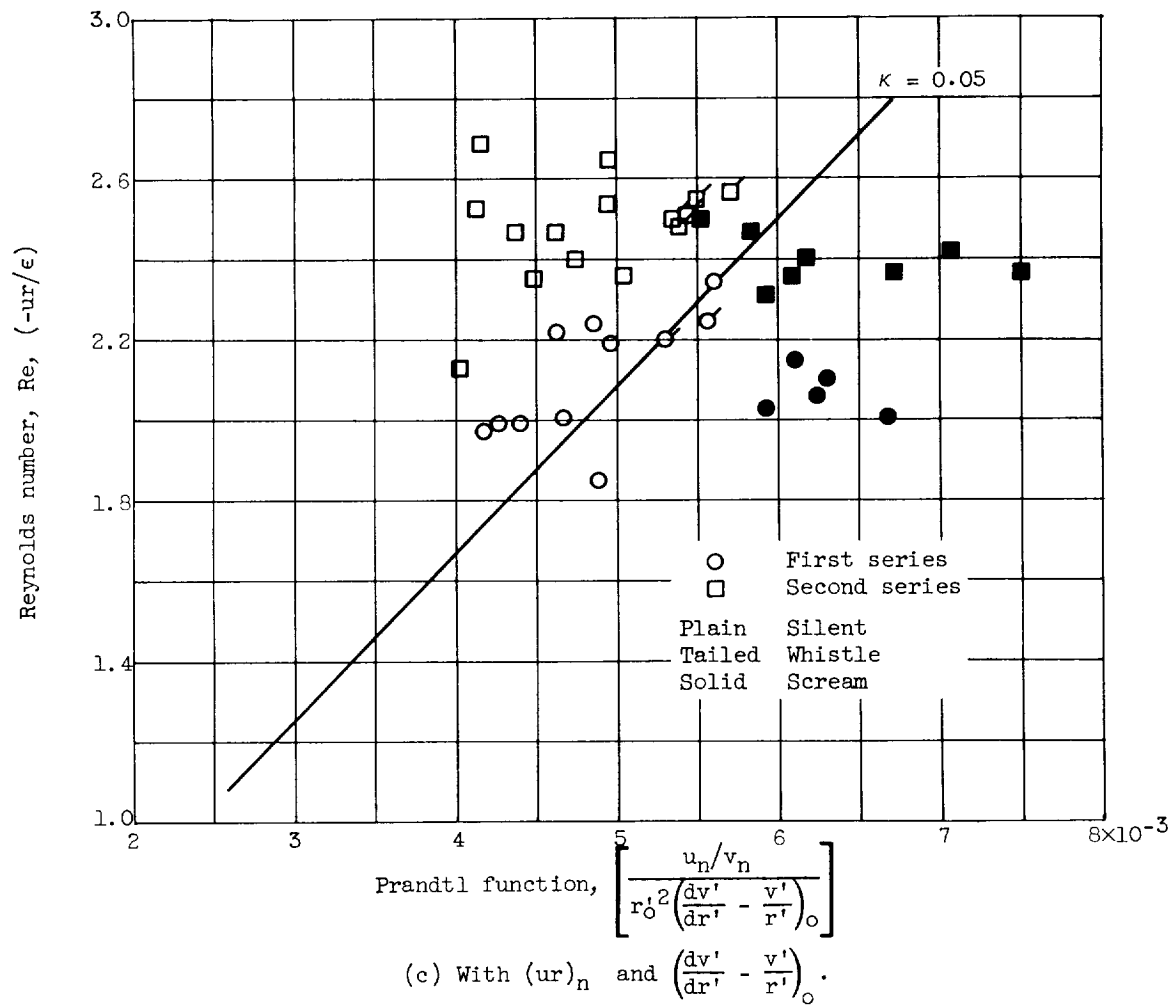
Figure 5. - Continued.   Prandtl function.
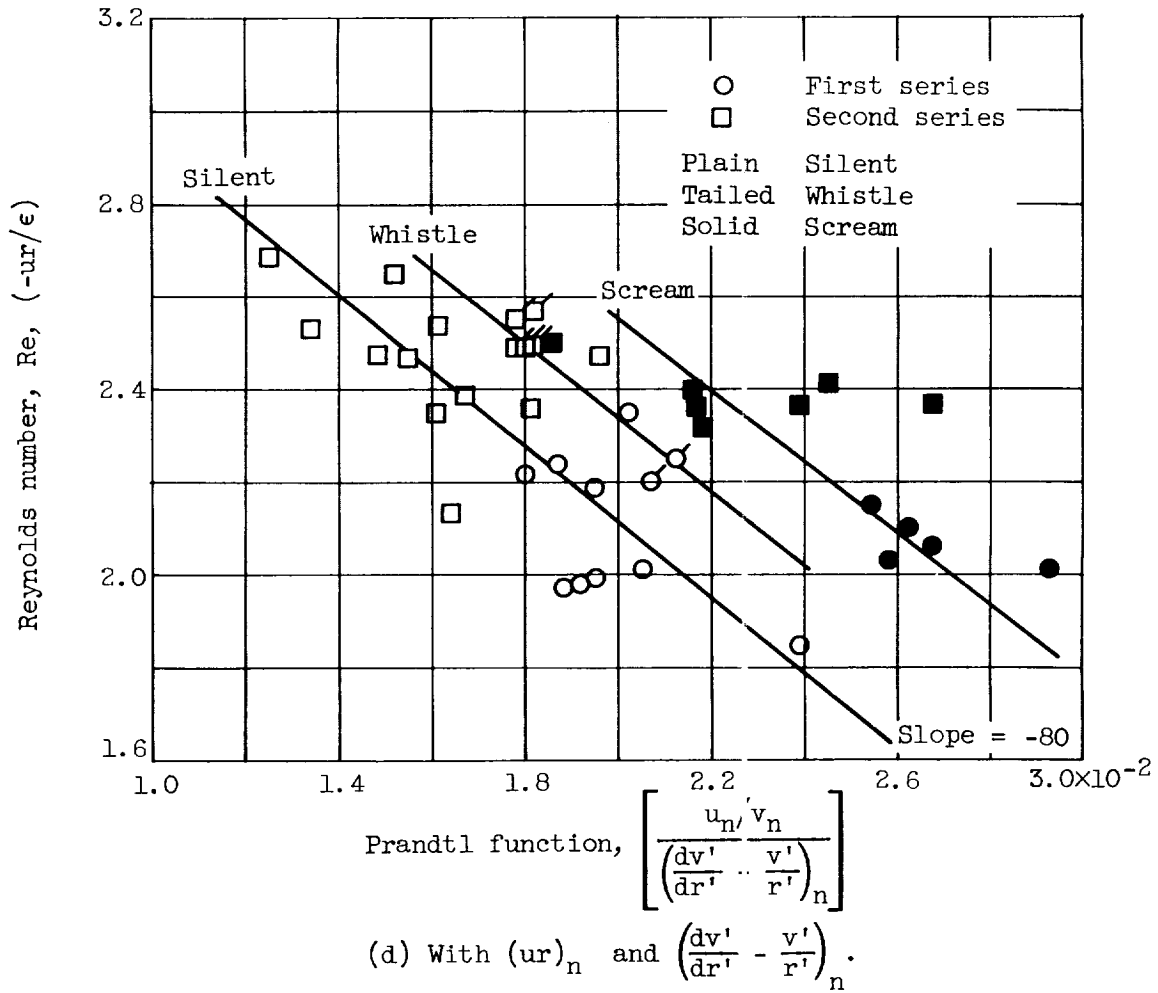
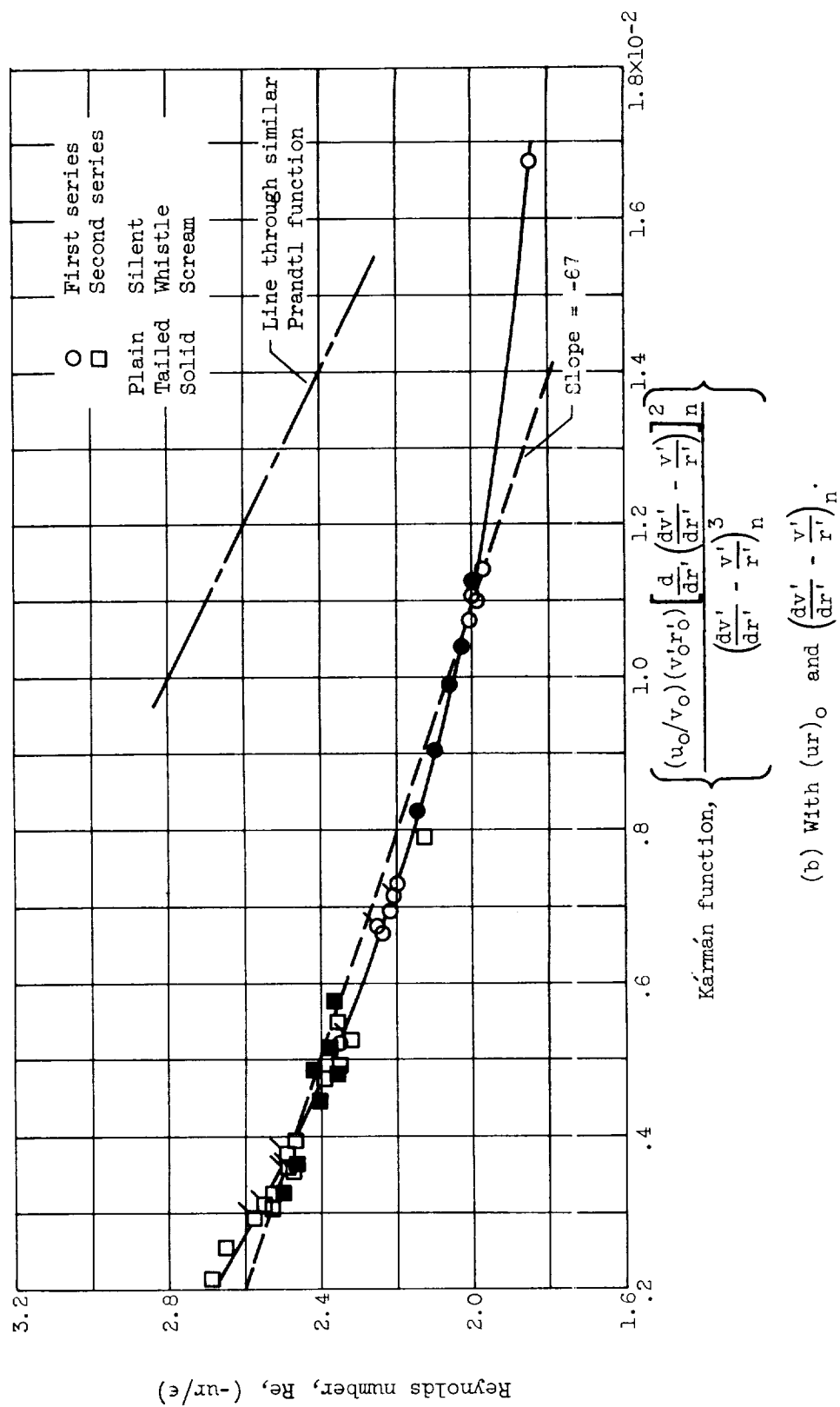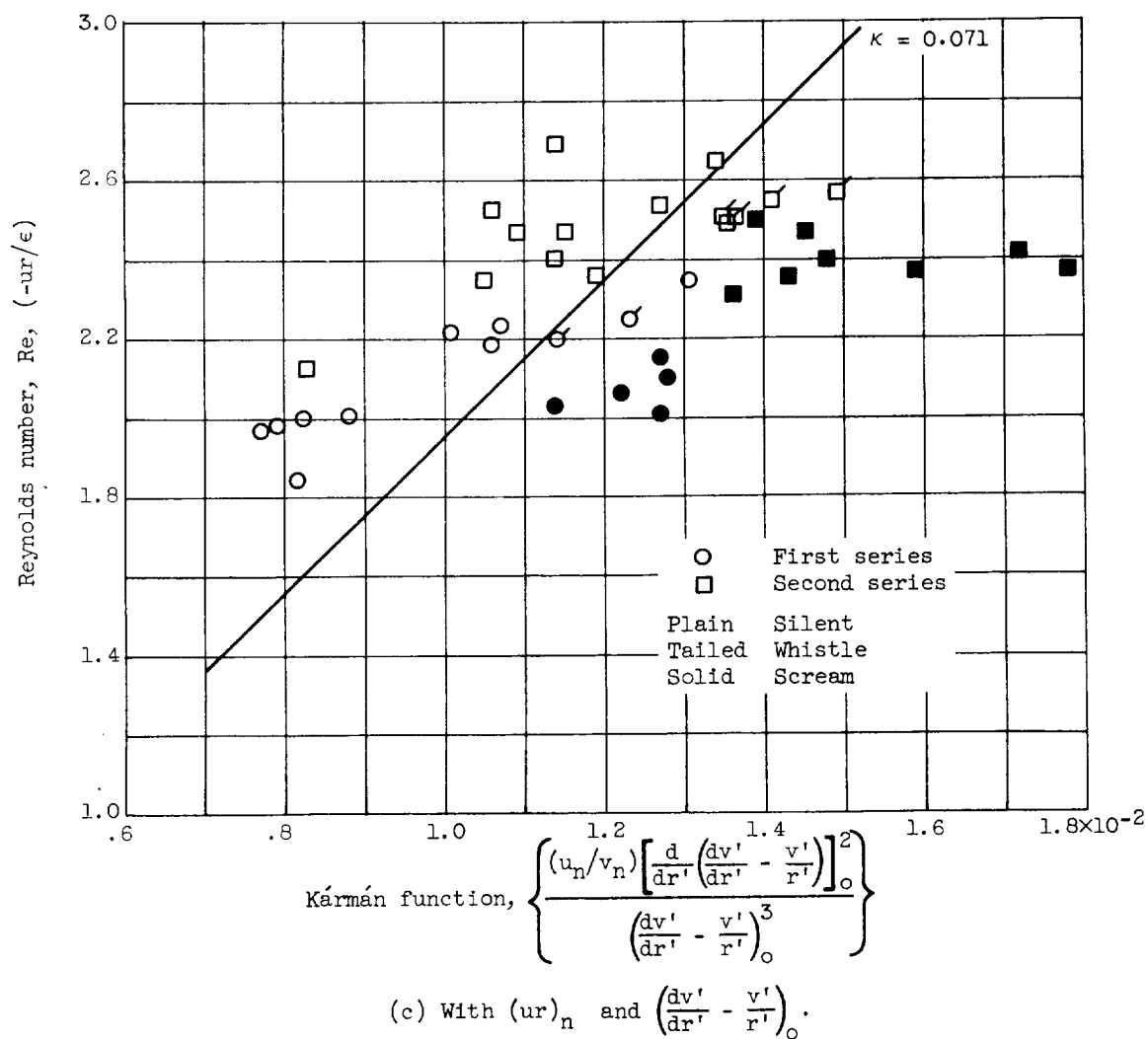Figure 5. - Concluded. Prandtl function.
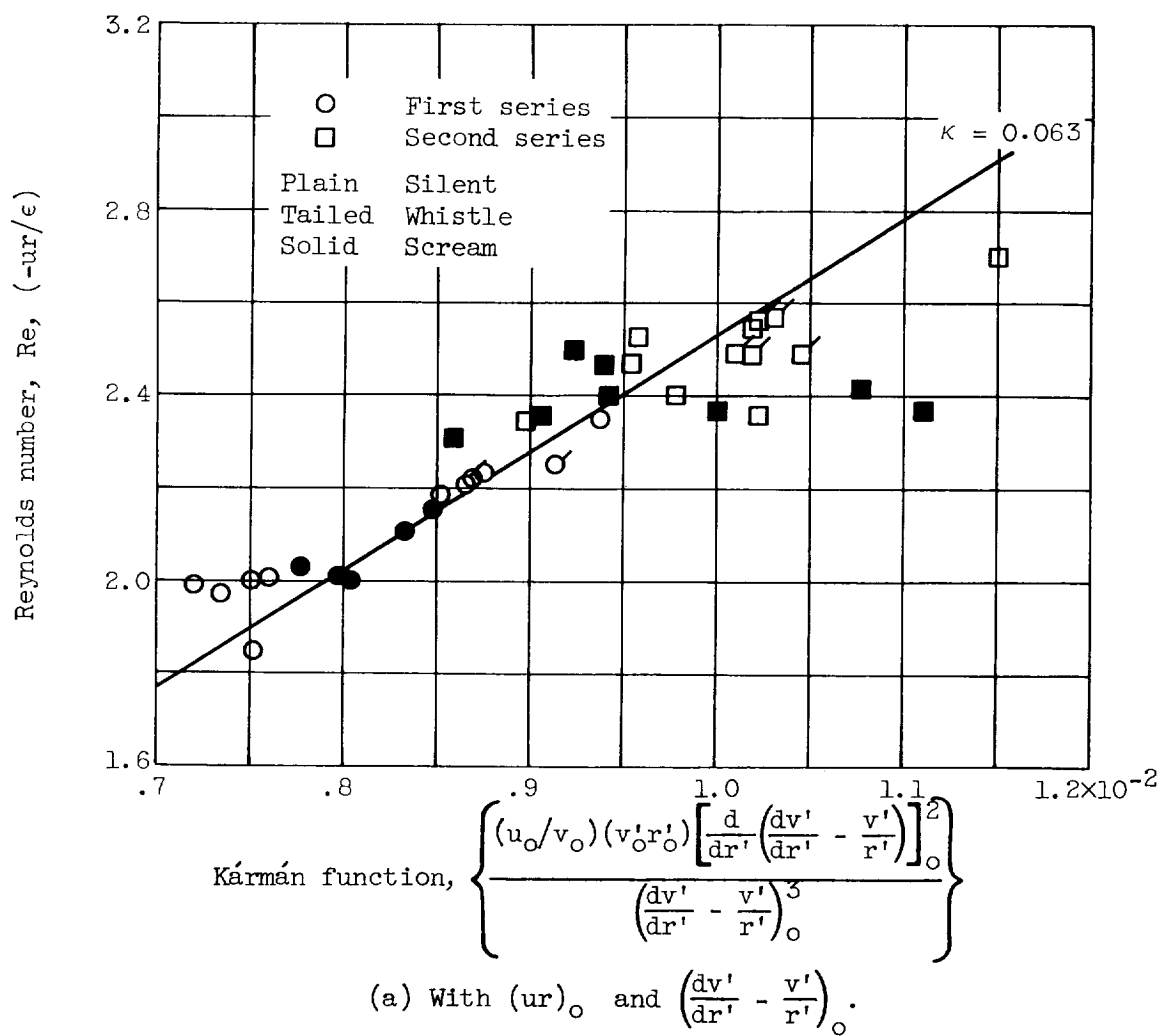
Figure 6. - Kármán function.

(b) With $(ur)_o$ and $\left(\dfrac{dv'}{dr'} - \dfrac{v'}{r'}\right)_n$.

Figure 6. - Continued. Kármán function.

(c) With $(ur)_n$ and $\left(\frac{dv'}{dr'} - \frac{v'}{r'}\right)_o$.

Figure 6. - Continued. Kármán function.

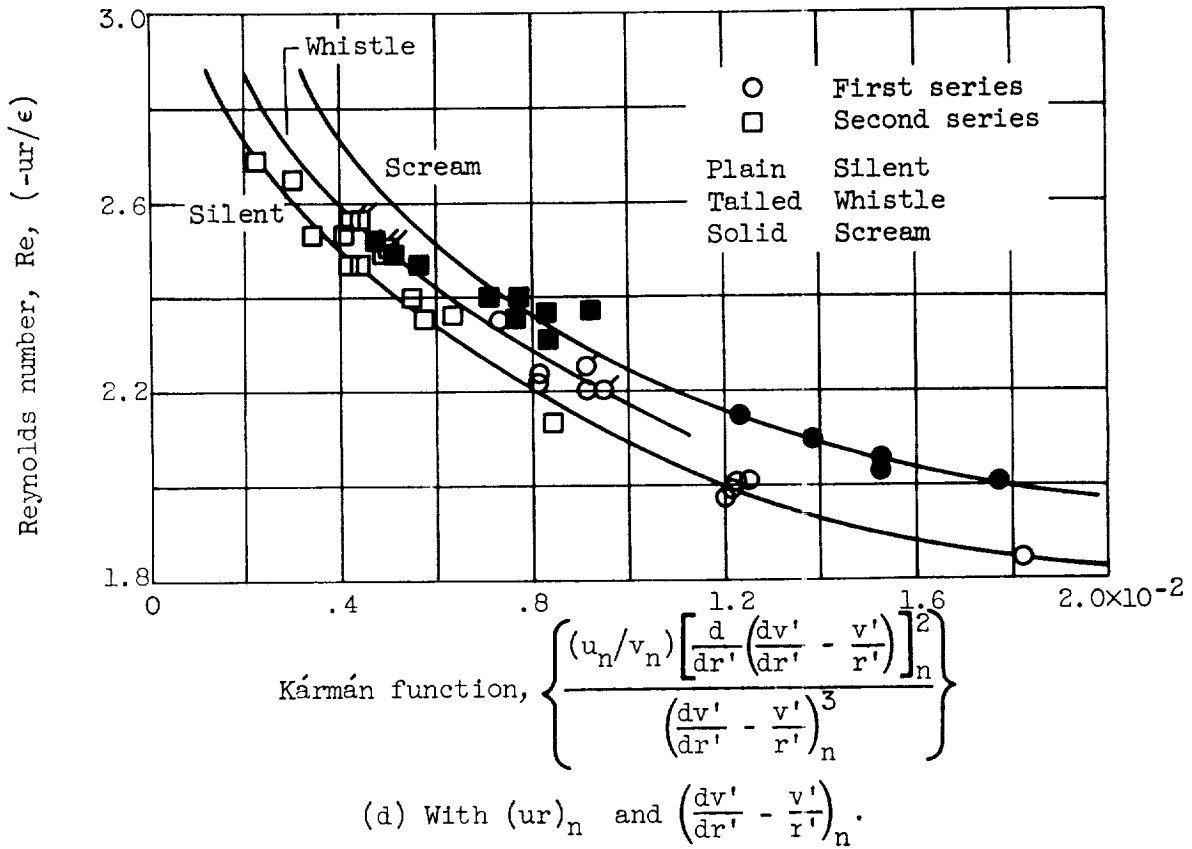(d) With $(ur)_n$ and $\left(\dfrac{dv'}{dr'} - \dfrac{v'}{r'}\right)_n$.
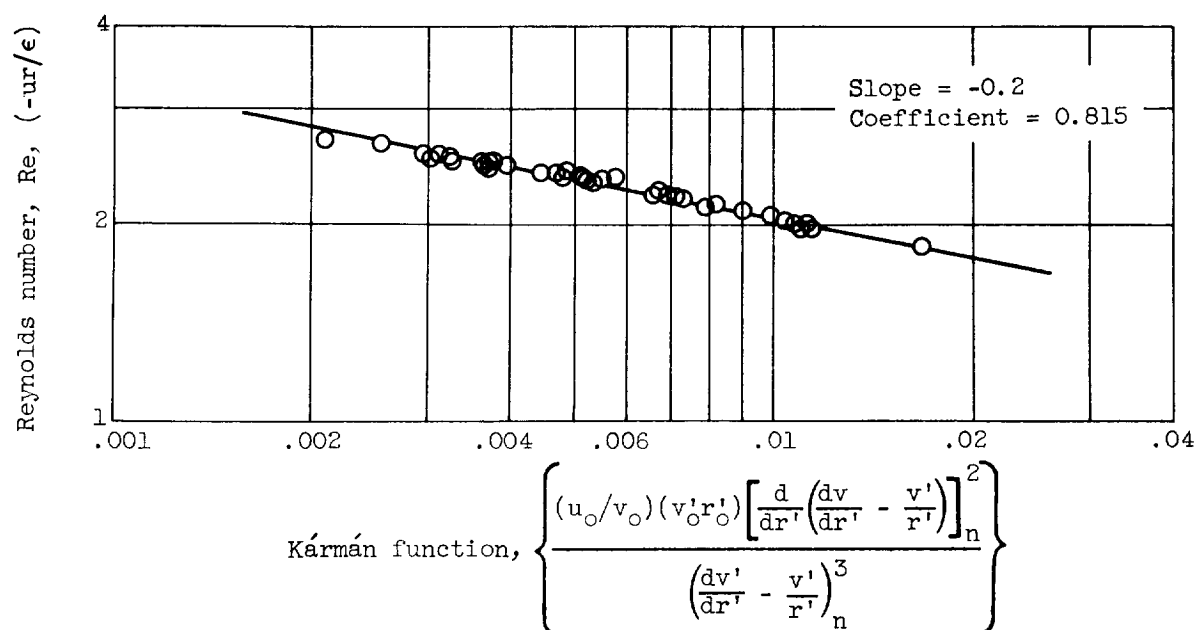
Figure 6. - Concluded. Kármán function.

Figure 7. - Plot of Kármán function with $(ur)_o$ and $\left(\dfrac{dv'}{dr'} - \dfrac{v'}{r'}\right)_n$ on log-log coordinates.